3. Experimental modal analysis of masonry buildings

In this chapter the experimental modal analysis and its application to masonry structures is analysed. In the last decades the advancement in sensor technologies and digital computation tools stimulated an extensive use of modal testing on cultural heritage objects. The first section is intended to present an accurate state-of-the-art analysis of linear system identification with particular emphasis on output-only techniques, which are known to be well-suited for architectural heritage buildings.

In the second section, model updating methods are introduced, and the importance of relying on a reference model for structural identification is also highlighted. A few examples are then presented on identification and model updating of significant cultural heritage structures.

3.1 System identification

3.1.1 Linear system identification and classification of methods

System identification refers to the development of structural models from input and/or output measurements performed on a real structure using sensing devices. Dynamic system identification is a major tool for the monitoring and the diagnosis of structures: in fact, experimental results from dynamic testing give knowledge about global structural behaviour and can be used in calibrating numerical models, in forecasting the response to dynamic and earthquake loading and can help in evaluating safety conditions [1,2,3].

Even if the age of virtual prototyping has already started [4], experimental testing and system identification are still playing a key role because they help the structural dynamicists to reconcile numerical predictions with experimental investigations. The term 'system identification' is sometimes used in a broader context in the technical literature and may also refer to the extraction of information about the structural behaviour directly from experimental data, i.e., without necessarily requesting a model (e.g., identification of the number of active modes or the presence of natural frequencies within a certain frequency range).

Linear system identification is a discipline that has evolved considerably during the last 30 years[5]. Experimental modal analysis is by all means the most popular

approach to performing linear system identification in structural dynamics. The model of the system is expressed in the form of modal parameters, namely the natural frequencies, mode shapes and damping ratios. The popularity of modal analysis stems from its great generality; modal parameters can describe the behaviour of a system for any input type and any range of the input.

Probably, the most common classification among identification methods is the one based on the domain where the method works. One can have methods working in:

- time domain;
- frequency domain;
- time-frequency domain.

A detailed description of method in these three domains will be performed in the next sections of this chapter.

The distinction among identification methods can be based also on the algorithm used. In fact, methods can be both direct and indirect. For what concerns direct methods, the identification process consists of determining the matrixes of the system model. Therefore, the mass, stiffness and damping matrixes of the dynamic equilibrium equations have to be determined. On the other hand, indirect methods are based on the Frequency Response Function (FRF) of the system and they estimate the modal parameters (natural frequencies, damping ratios, amplitude and phase of the modal shapes).

A further classification can be made by resorting to the number of modes considered by the identification technique:

- single degree of freedom (SDOF) analysis.
- multi-degree of freedom (MDOF) analysis.

For instance in the frequency domain one can work both with SDOF or MDOF analysis, while in the time domain and with direct method only MDOF algorithms are available.

Another typical classification is the one based on the number of input and output channels. The type of system depends mostly on the number of sensors available, for what concerns output channels, and on the type of excitation used, for what concerns input channels. Identification methods can be framed in four classes:

- SISO (single input-single output): only one point of the system is excited and only one FRF can be determined.
- SIMO (single input-multiple output): only one point of the system is excited but many FRFs can be determined.
- MISO (multiple input-single output): these class of method is less common than the others, in this case several points of the system are excited and the output is read in only one point.
- MIMO (multiple input-multiple output): in this case multiple points of the system are excited and the output is measured in multiple points of the system.

Finally, a last distinction can be made on the basis of the source of excitation used in the identification process. In fact one can have an excitation known (such in the case of an impulse, excitation through a vibrodyne or a shaker) or unknown (environmental noise, wind, traffic…).

For a description and classification of various input-output modal analysis techniques the reader may consult specialized texts [3,6,7].

3.1.2 Time domain methods

In recent years, time domain techniques have been used rather successfully, thanks to the great spectral resolution offered and to their modal uncoupling capability [8,9,10,11,12,13]. One of the basic shortcomings of these methods is that they often produce spurious modes, whose true nature, however, can usually be identified by means of simple modal form correlation indicators [6], or, as an alternative, with the aid of numerical models.

An important family of time domain methods makes use of time series autoregressive models and exploits the theoretical results coming from research in the field of system control [14]. These techniques provide a very general and attractive formulation, and are frequently applied to civil structures. The most critical aspect resides in the computational complexity associated with applications to multi-degree-of-freedom (M-DOF) systems. The extension of the parameter estimation techniques to stochastic multi-variate models, in fact, is far from being trivial, and additional difficulties arise from local minimum points and algorithmic instabilities [15].

Among the deterministic methods, in addition to the historic Ibrahim Time Domain [16], we should mention the Eigensystem Realisation Algorithm (ERA) [17], which, based on a Single Value Decomposition (SVD) of Hankel's matrix, has been closely studied in the literature (e.g. [18]), and the Polyreference Time Domain (PRTD) stemming from a generalisation of Prony's method [19,20].

Since the beginning of the Nineties, there has been an increasing interest in so-called Stochastic Subspace Identification methods, in which statistical, algebraic and numerical concepts and algorithms cooperate, leading to user-friendly software for linear system identification [12,21,22]. Contrary to classical algorithms, subspace algorithms do not suffer from the problems caused by a-priori parameterisations and non-linear optimizations. Van Overschee and De Moor [23] studied three different subspace algorithms for the identification of combined deterministic-stochastic systems. This comparison is done through the introduction of a unifying theorem, of which the three algorithms are special cases.

3.1.2.1 Autoregressive methods

Let us write the 2nd order dynamic equilibrium equation for a linear system with N degrees of freedom at the discrete time $t_k = k \cdot \Delta t$, through an autoregressive moving average model [3,14]:

$$\{x_k\} = [a_1]\{x_{k-1})\} + \ldots + [a_n]\{x_{k-n}\} + [b_0]\{u_k\} + [b_1]\{u_{k-1}\} + \ldots + [b_{n-1}]\{u_{k-n-1}\} + \{e_k\} \quad (3.1)$$

in this expression $\{x\}$ is the vector of displacements, $\{u\}$ is the input vector, matrices $[a]$ represent the autoregressive part, whilst matrices $[b]$ represent the moving average part, vector $\{e_k\}$ represents the prediction error taking into account noise. Index n represents the order of the model (in linear dynamics $n \geq 2$). By reproducing (3.1) for L subsequent instants we can arrange the L resulting equations in a compact form [3,24]:

$$[x]=[\vartheta]\cdot[Y]+[e] \tag{3.2}$$

where

$$\underset{(NxL)}{\left[\{x(n+1)\} \quad ... \quad \{x(n+L)\}\right]}$$

$$[\vartheta]=\left[[a_1] \quad ... \quad [a_n] \quad [b_0] \quad ... \quad [b_{n-1}]\right] \tag{3.3}$$

$$[Y]=\underset{((Nn+qn)xL)}{\begin{bmatrix} \{x(n)\} & ... & \{x(n+L-1)\} \\ ... & ... & ... \\ \{x(1)\} & ... & \{x(L)\} \\ \{u(n+1)\} & ... & \{u(n+L)\} \\ ... & ... & ... \\ \{u(2)\} & ... & \{u(L+1)\} \end{bmatrix}} \tag{3.4}$$

$$\underset{(NxL)}{\left[\{e(n+1)\} \quad ... \quad \{e(n+L)\}\right]} \tag{3.5}$$

The minimisation of the error, $[e]^T[e]$, yields an estimate of matrix $[\vartheta]$:

$$[\vartheta]=[x]\cdot[Y]^T\left([Y]\cdot[Y]^T\right)^{-1}=[x]\cdot[Y]^+ \tag{3.6}$$

where $[Y]^+$ indicates the pseudo-inverse of matrix $[Y]$.

In unknown input conditions, we can start with the construction of a purely autoregressive model (AR) [25]:

$$[x]=[\vartheta_R]\cdot[Y_R]+[u] \tag{3.7}$$

$$\begin{aligned}
\underset{(NxL)}{[x]} &= \left[\{x(n+1)\} \quad ... \quad \{x(n+L)\} \right] \\
\underset{(NxNn)}{[\vartheta_R]} &= \left[[a_1] \quad ... \quad [a_n] \quad [b_0] \quad ... \quad [b_{n-1}] \right]
\end{aligned} \tag{3.8}$$

$$\underset{(NnxL)}{[Y]} = \begin{bmatrix} \{x(n)\} & ... & \{x(n+L-1)\} \\ ... & ... & ... \\ \{x(1)\} & ... & \{x(L)\} \end{bmatrix} \tag{3.9}$$

$$\underset{(NxL)}{[u]} = \left[\{u(n+1)\} \quad ... \quad \{u(n+L)\} \right] \tag{3.10}$$

Based on the initial estimate of $[\theta_R]$ and the ensuing evaluation of $[f]$ by difference from (3.7) we can perform a new least square minimisation for the determination of $[\theta]$. Eigenvalues and eigenvectors are calculated accordingly [3].

3.1.2.2 Eigensystem Realisation Algorithm (ERA) applied to Random Decrement (RD) signatures

Dynamic response signals contain two parts: a free decay component due to the system's initial state and a component associated with the forced response. Given a random stationary response signal with zero mean and even probability density distribution, let us select a set of points that satisfy a specific triggering condition. Each chosen point may be viewed as the initial state of a signal sequence. The average among a large number of sequences will converge to a system's free decay signature.

The auto and cross RD transforms are defined as the average values of the realisations of a stochastic process, after a delay τ from the instant when a particular "triggering condition" is satisfied. In practical applications, the triggering condition mainly used is the "positive point" one. The reason is that the correlation functions or their derivatives are often searched alternatively [26].

The RD technique is often used in conjunction with identification methods based on impulse response, as the latter is directly related to the correlation function [26,27]. An impulse response based technique most commonly studied and employed with RD functions is based on the Eigenvalue Realization Algorithm (ERA), as described below.

The state space formulation (1st order equilibrium equation) associated to (3.1) can be written in the discrete time form as follows [3,17]:

$$\{X_{k+1}\} = [A]\{X_k\} + [B]\{\delta_k\} \qquad k = 0,1,2,... \tag{3.11}$$

where $\{X_k\}$ represents the state vector, and $\{\delta_k\}$ stands for impulse excitation. Assuming that at the initial time it is $\{u_0\}=\{0\}$ and knowing that $\{\delta_0)\}=\{1,0,...0\}^T$ and $\{\delta_k\}=\{0\}$ at $k > 0$, and by considering all loading points, for all subsequent time intervals we can write:

$$[Y_k]=[A]^{k-1}[B] \qquad k>0 \tag{3.12}$$

The k Markov parameters $[Y_k]$, which represent the measured signals (or their RD functions when working with ambient measurements) can be organised in a Hankel matrix. Some conditions are to be met for obtaining a sufficient quantity of data to perform a Single Value Decomposition (SVD) on the Hankel matrix [28].

$$\left[W\right]=\left[[B] \quad [A][B] \quad ... \quad [A]^{s-1}[B]\right] \tag{3.13}$$

This process is known as realisation and it entails the determination of the [A] and [B] matrices from redundant data.

There are an infinite number of sets of matrices that satisfy (3.12) since there are an infinite number of realisations for the system; the aim is to obtain the realisation which, while giving origin to the state space formulation with the lowest degree, still represents the dynamic behaviour of the structure. The system's modal parameters are obtained by extracting the eigenvalues and eigenvectors from the realised matrix [A].

3.1.2.3 Stochastic Subspace Identification (SSI) method

When ambient excitation is considered, the input is unmeasured and equation (3.11) becomes:

$$\{X_{k+1}\}=[A]\{X_k\}+\{e_k\} \qquad k=0,1,2,... \tag{3.14}$$

The SSI method requires the assumption that $\{e_k\}$ is constituted by white noise. If this assumption is violated, the main frequencies contained in the input signals cannot be separated from the authentic modal components, when solving the eigenvalue problem.

Conceptually, SSI methods start by building large block Hankel matrices from the output sequence, divided up in 'past' and 'future' data matrices [23]. The Kalman filter state sequence can be obtained by projecting the row space of the future block Hankel matrix, into the row space of the past block Hankel matrix. This can be done using the concept of angles between subspaces, which is a generalization of the angle between two vectors. Once that state sequence is obtained, the estimation of the system's characteristic matrices follows from solving a least squares problem.

The technique implemented here is the third algorithm considered in the unifying theorem by Van Overschee and DeMoor [23]. This method is often referred to as the "Canonical Variate Analysis" (CVA) and is due to Larimore [29]. It is based on statistical

arguments and makes extensive use of principal angles and directions. The reader is referred to the references for details.

3.1.3 Frequency domain methods

Frequency domain methods tend to perform better when the frequency range and the number of modes are limited. Methods in the frequency domain were the first to be used in the field of identification but problems related to the resolution in frequency, leakage phenomena [3] or high modal density, led to the introduction of time-domain based algorithms.

Anyway, especially in the field of masonry structures several examples of frequency domain methods are available. For instance, Capecchi e D'Ambrogio [30] use a modified version of the method of "Rational Fraction Polynomial (RFP)" [31] together with the Hilbert transform in order to eliminate the non-linear contribution, to identify an old masonry building. Genovese *et al* [32] and Beolchini and Antonacci [33] used the Goyder's method [34] in order to approximate the experimental frequency response functions with a least square minimisation and using a different set of function with respect to the RFT method. A common situation in experimental analysis is the identification of signal with unknown excitation, in such a case spectral method have been often applied [35,36,37,38,39].

Nowadays, one of the most common and applied methods of identification in the frequency domain is the Frequency Domain Decomposition (FDD), also due to the availability of simple commercial codes. The FDD method [40] can be viewed as an extension of the traditional basic frequency domain method. It is performed using the output power spectral density (PSD), and based on the assumption that the excitation is pure Gaussian white noise and that all natural modes are lightly damped [40]. A singular value decomposition (SVD) is carried out for each PSD matrix and all modes contributing to the vibratory signature of a structure at a given frequency are separated into principal values and orthogonal vectors. When a single mode identified by peak picking at a given frequency prevails in the spectrum, the first vector obtained by the SVD will constitute an estimate of the mode shape. The first singular value corresponding to this mode should be approximately equal to the sum of the terms on the diagonal of the PSD matrix, which means that most of the power of the measured signals at this frequency can be attributed to the vibratory signature of this particular mode. Other singular values that are not associated with any mode will consist of decomposed noise initially contained in the signals before the SVD was performed.

Once natural frequencies have been roughly identified by peak picking and mode shapes have been estimated using the singular vector matrices, equivalent single degree of freedom 'spectral bells' are identified for each mode. This step is achieved by comparing the estimated mode shape of interest with all vectors previously estimated throughout the spectrum by SVD of all the PSD matrices. A comparison of the mode shapes is then carried out by computing the modal assurance criterion (MAC - see section 3.2.4). All singular values corresponding to a MAC value superior to a user-specified parameter (which is called the MAC rejection level) are kept, thus forming an equivalent single degree of freedom spectral bell. Then, by inverse fast Fourier transform (IFFT) of that spectral bell, the resulting auto-correlation function can be used to revaluate the

frequency by counting the number of zero crossings in a finite time interval. Damping ratios are also estimated using the logarithmic decrement of the auto-correlation function.

3.1.4 Time-frequency domain methods

The main advantage of time-frequency domain analysis is its ability to handle non-stationary waveform signals, which are very common when structural damage and faults occur.

As an example, let us consider a signal that features a time localization of spectral components. The Fourier transform is not suited for the analysis of such components, since it projects the signal on infinite harmonics which are not localized in time. If at any time instant only a single frequency is present, an instantaneous frequency may be variously defined; this quantity is commonly identified with the rate of phase change in the analytic signal [41]. Such a definition is capable of describing the time localization of a specific class of signals, but proves to be unsuitable for multi-component ones.

In all cases where mono-dimensional representations are inadequate one can turn to bi-dimensional (joint) functions $T_x(t, f)$ of the variables time and frequency. $T_x(t, f)$ is referred to as "time frequency representation" (TFR) of the signal $x(t)$.

3.1.4.1 Linear time-frequency transforms

3.1.4.1.1 Short Time Fourier Transform (STFT)

In order to introduce the time localization of frequency components, a simple solution is obtained by pre-windowing the signal around a particular time *t*, as shown in Figure 1, calculating its Fourier transform, and doing that for each time instant *t*. Accordingly, the "short-time Fourier transform" (STFT), of a signal $x(t')$ is defined as [42]:

$$STFT_X^{(\gamma)}(t, f) = \int_{-\infty}^{+\infty} x(t')\ \gamma^*(t - t')\ e^{-j2\pi ft'}\ \mathrm{d}t' \tag{3.15}$$

where $\gamma(t)$ is a short time analysis window centred around *t*. The superscript * denotes complex conjugation.

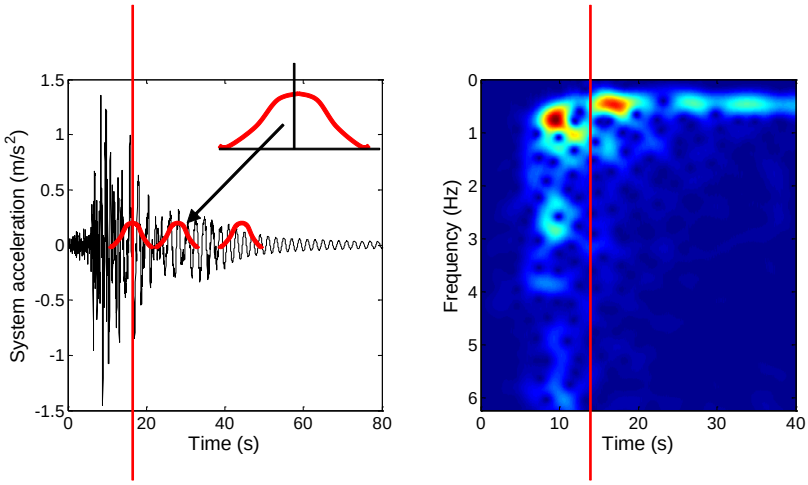

Figure 3.1 - Prewindowing of a signal in the time domain and time-frequency representation.

Since multiplication by the relatively short window $\gamma(t'-t)$ effectively suppresses the signal outside a neighbourhood around the analysis time point $t'=t$, the STFT is a "local" spectrum of the signal $x(t')$ around t.

The STFT is evidently linear and is complex-valued in general. Provided that the short-time window is of finite energy, the STFT is invertible through:

$$x(t)=\int_{-\infty}^{+\infty}\int_{-\infty}^{+\infty} STFT_X^{(\gamma)}(t',f')\, g(t-t')\, e^{j2\pi f' t}\cdot \mathrm{d}t'\cdot \mathrm{d}f' \tag{3.16}$$

with $\int g(t)\gamma^*(t)\mathrm{d}t=1$. Equation (3.16) implies that the total signal can be decomposed as a weighted sum of elementary waveforms:

$$g_{t,f}(t')=g(t'-t)\cdot e^{j2\pi ft'} \tag{3.17}$$

which can be interpreted as "atoms". Each atom is obtained from the window $g(t)$ by a shift in time and in frequency (modulation).

The STFT may also be expressed in terms of signal and window spectra:

$$STFT_x^{(\gamma)}(t,f)=\int_{-\infty}^{+\infty} X(f')\,\Gamma^*(f'-f)\, e^{j2\pi(f'-f)t}\, \mathrm{d}f' \tag{3.18}$$

where X and Γ are respectively the Fourier transform of x and γ. Accordingly, the STFT can be interpreted as the result of passing the signal through a filter with frequency

response $\Gamma(f'-f)$ and is therefore deduced from a mother filter $\Gamma(f)$ by a translation of f. The STFT is thus similar to a bank of band-pass filters with constant bandwidth.

The STFT preserves time-frequency shift (see property P3 in Table 1). Such transform, as well as its squared magnitude, the "Spectrogram" (SPEC), is frequently used in many application fields, including modal decoupling, system identification (e.g. [43,44]), group velocity, speech recognition etc.

The time resolution of the STFT can be obtained by considering for x a Dirac impulse:

$$x(t)=\delta(t-t_0) \qquad \Rightarrow STFT_x^{(\gamma)}(t,f)=e^{-j2\pi ft_0}\ \gamma(t-t_0) \tag{3.19}$$

Thus, the time resolution of the STFT is proportional to the effective duration of the analysis window γ. Similarly, to obtain the frequency-resolution, we have to consider a complex sinusoid (an impulse in the frequency domain):

$$x(t)=e^{j2\pi f_0 t} \qquad \Rightarrow STFT_x^{(\gamma)}(t,f)=e^{-j2\pi f_0 t}\ \Gamma(f-f_0) \tag{3.20}$$

hence the frequency-resolution of the STFT is proportional to the effective bandwidth of the analysis window γ. As a consequence, for the STFT, we have a "trade-off" between time and frequency resolutions: while a good time resolution requires a short window γ, a good frequency resolution requires a narrow-band filter i.e. a long window. This limitation is a consequence of the Heisenberg-Gabor inequality [41,45]:

$$T\cdot B\geq 1 \tag{3.21}$$

where T is the signal's temporal length and B is the bandwidth. The lower bound of the product is reached for Gaussian functions.

3.1.4.1.2 Discrete STFT

Equation (3.15) can be sampled on a rectangular grid:

$$STFT_x^{(\gamma)}(n,m)=STFT_x^{(\gamma)}(nt_0,mf_0)=\int_{-\infty}^{+\infty}x(t')\ \gamma^*(t'-nt_0)\ e^{-j2\pi mf_0t'}\mathrm{d}t' \tag{3.22}$$

where n and m are integers.

The problem is then to choose the sampling period t_0 and frequency f_0 so as to minimize the STFT inherent redundancy without losing any information [46]. For a sampled signal $x[n]$ whose sampling period is noted Δt, t_0 has to be chosen as a multiple of Δt such that $t_0\cdot f_0\leq 1$. We then have the following analysis and synthesis formulae:

$$STFT_x^{(w)}[n,m] = \sum_k x[k] \cdot \gamma^*[k-n] \cdot e^{-j \cdot 2\pi \cdot mk} \quad \text{for } -1/2 \le m \le 1/2 \tag{3.23}$$

$$x[k] = \sum_n \sum_m STFT_x^{(w)}[n,m] \cdot g[k-n] \cdot e^{j \cdot 2\pi \cdot mk} \tag{3.24}$$

Equations (3.23)-(3.24) can be implemented efficiently by means of overlap "fast Fourier transform" (FFT) techniques.

Alternatively, a filter-bank implementation is possible, based on sampling equation (3.18).

3.1.4.1.3 Wavelet transform

Another important TFR is the time-frequency version of the Wavelet transform (WT) defined as [42,47]:

$$WT_x^{(\psi)}(t,f) = \int_{t'} x(t') \cdot \sqrt{\left|\frac{f}{f_c}\right|} \cdot \psi^*\left(\frac{f}{f_c}(t'-t)\right) \cdot \mathrm{d}t' \tag{3.25}$$

where $\psi(t)$ is a real or a complex band-pass function centred around $t=0$ in the time domain. The parameter f_c in equation (3.25) corresponds to the centre frequency of $\psi(t)$. The WT was originally introduced as a time-scale representation and in fact retains the important property of preserving time shifts and time scaling. It does not, however, preserve frequency shifts.

The WT's time and frequency resolutions are related via the Heisenberg-Gabor inequality, like in the STFT case. However, while the STFT's resolution is the same for each analysis frequency, the WT's frequency resolution (respectively time resolution) becomes poorer (respectively better) as the analysis frequency grows.

Scale shift invariance makes the WT, or its squared magnitude, the "Scalogram" (SCAL), a frequent choice in pattern recognition and many other application fields, including ridge and phase estimation (e.g. [48,49]) and SHM (e.g. see the list of references in [50,51]).

3.1.4.2 Quadratic time-frequency transforms

Although linearity is a desirable property, quadratic TFRs [42,52] allow for interpreting the distributions from an energy point of view. This interpretation is expressed by the so-called "marginal properties":

$$\int_{-\infty}^{+\infty} T_x(t,f)\mathrm{d}f = |x(t)|^2; \quad \int_{-\infty}^{+\infty} T_x(t,f)\mathrm{d}t = |X(f)|^2 \tag{3.26}$$

having defined the "instantaneous power" $\left|x(t)\right|^2$ and the "spectral energy density" $\left|X(f)\right|^2$. Consequently the signal energy is:

$$E_x = \int_{-\infty}^{+\infty} \left|x(t)\right|^2 \mathrm{d}t = \int_{-\infty}^{+\infty} \left|X(f)\right|^2 \mathrm{d}f = \int_{-\infty}^{+\infty}\int_{-\infty}^{+\infty} T_x(t,f)\,\mathrm{d}t\mathrm{d}f \tag{3.27}$$

The marginal properties are not sufficient to identify an energy density at every point in the time-frequency plane, since the uncertainty principle does not allow such a notion. Vice-versa, many quadratic TFRs may loosely support an energetic interpretation even if they do not satisfy the marginal properties, among them the SPEC and the SCAL:

$$SPEC_x^{(\gamma)}(t,f) = \left|STFT_x^{(\gamma)}(t,f)\right|^2 \tag{3.28}$$

$$SCAL_x^{(\psi)}(t,f) = \left|WT_x^{(\psi)}(t,f)\right|^2 \tag{3.29}$$

In equation (3.28) the linearity structure of the STFT is violated, and in fact any quadratic TFR satisfies the "quadratic superposition principle":

$$\begin{aligned} &x(t) = c_1 x_1(t) + c_2 x_2(t) \Rightarrow \\ &T_x(t,f) = \left|c_1\right|^2 T_{x_1}(t,f) + \left|c_2\right|^2 T_{x_2}(t,f) + \\ &\quad + c_1 c_2 T_{x_1 x_2}(t,f) + c_2 c_1 T_{x_2 x_1}(t,f) \end{aligned} \tag{3.30}$$

The last two terms in equation (3.30) are the cross-terms or interference terms. The interference terms are oscillatory structures which are restricted to those regions of the time-frequency plane where the auto-terms (or authentic terms) overlap. In the specific cases of the SPEC and the SCAL, if two components are sufficiently far apart in the time-frequency plane, then their interference terms will be virtually nil.

Quadratic representations have recently served as an effective tool in structural diagnostics and machine fault detection [50,51].

3.1.4.2.1 The autocorrelation form and the Wigner-Ville transform

A general approach to deriving time-dependent spectra is by generalizing the Wiener-Khinchine theorem: the correlation function and the power spectrum form Fourier transform pair. By assuming the symmetric form for the instantaneous temporal and spectral autocorrelation, which are also functions of the time lag τ and the frequency lag ν, respectively

$$r_x(\tau,t) = x(t-\tau/2)x(t+\tau/2) \tag{3.31}$$

$$r_x(\tau,t) = X(f-\nu/2)X(f+\nu/2) \tag{3.32}$$

and by transforming equations (3.31) and (3.32) one obtains [41]:

$$\begin{aligned} W_x(t,f) &= \int_{-\infty}^{+\infty} x(t+\tau/2)x^*(t-\tau/2)e^{-j2\pi f\tau}\mathrm{d}\tau \\ &= \int_{-\infty}^{+\infty} X(f+\nu/2)X^*(f-\nu/2)e^{j2\pi t\nu}\mathrm{d}\nu \end{aligned} \tag{3.33}$$

Equation (3.33) gives the "Wigner distribution" (WD), a transformation well known in quantum mechanics, whose signal processing version is often referred to as Wigner-Ville distribution.

By taking the instantaneous cross-correlation between two signals, $x_1(t)$ and $x_2(t)$, the WD assumes the following more general form:

$$\begin{aligned} W_{x_1x_2}(t,f) &= \int_{-\infty}^{+\infty} x_1(t+\tau/2)x_2^*(t-\tau/2)e^{-j2\pi f\tau}\mathrm{d}\tau \\ &= \int_{-\infty}^{+\infty} X_1(f+\nu/2)X_2^*(f-\nu/2)e^{j2\pi t\nu}\mathrm{d}\nu \end{aligned} \tag{3.34}$$

The WD satisfies a large number of desirable properties (see Tables 1-2), in particular marginals, shift invariance and real-valuedness. The instantaneous frequency [41] and the group delay can be evaluated using the local first-order moments of the WD [1].

Among the dual class of correlative TFRs, which combine temporal and spectral correlations, an important role is played by the "ambiguity function" (AF) [42]:

$$\begin{aligned} A_{x_1,x_2}(\tau,\nu) &= \int_{-\infty}^{+\infty} x_1(t+\tau/2)x_2^*(t-\tau/2)e^{-j2\pi\nu t}\mathrm{d}t \\ &= \int_{-\infty}^{+\infty} X_1(f+\nu/2)X_2^*(f-\nu/2)e^{j2\pi\tau f}\mathrm{d}f \end{aligned} \tag{3.35}$$

The AF may be viewed as a joint time-frequency correlation function. Along $\nu = 0$ and $\tau = 0$ axes AF reduces to the time correlation function and the frequency correlation function, respectively (correlative marginal properties).

3.1.4.3 Cohen class of transforms

Among quadratic transforms, those belonging to the Cohen (or shift-invariant) class are characterized by the invariance of its members to time and frequency shifts (see P2 in Table 1), a property that is desirable for correlating the signal characteristics to phenomena that take place in the mechanical system which generates the signal. Cohen demonstrated that every member of the shift-invariant class is a filtered version of the WD, and that it is possible to use a general formula for describing all of them [1]. Indeed, equivalent formulas can be written in four different domains: temporal correlation domain (t,τ), time-frequency domain (t,f), ambiguity function domain (τ,ν), spectral correlation domain (ν,f) [53,54]. For instance, the following relation holds in the temporal correlation domain:

$$T_x(t,f)=\int_{-\infty}^{+\infty}\int_{-\infty}^{+\infty} r_x(t',\tau)\varphi(t-t',\tau)e^{-j2\pi f\tau}\mathrm{d}t'\mathrm{d}\tau$$
$$\varphi(t,\tau)=\int_{-\infty}^{+\infty} g(\nu,\tau)e^{-j2\pi\nu t}\mathrm{d}\nu \tag{3.36}$$

where $g(\nu,\tau)$ is the kernel that uniquely identifies the specific TFR ($g(\nu,\tau)=1$ for the WD).

3.1.4.4 Desirable properties of the t-f distributions

A standard set of desirable properties is usually referred [41,42,54] to compare the performance of different transforms. Herein, we consider a subset which contains the main characteristics that are of interest in the application context under discussion. In table 3.1 properties are related to the corresponding requirements on the kernel. Table 3.2 reports the properties of eight important shift-invariant transforms, including the SPEC. The SPEC is in fact a member of Cohen's class, but, since it does not offer independence of temporal and spectral resolutions, it is generally classed as linear [41]. It is worthy to note that only the SPEC satisfies P0, while sacrificing non-negativity is mandatory in order to gain time-frequency resolution.

	PROPERTY	**CONDITION ON THE KERNEL**
P0	Non-negativity: $T_x(t,f)\geq 0 \quad \forall t \quad \forall f$	$g(\nu,\tau)$ is the AF of some $f(t)$
P1	Realness: $T_x(t,f)=T_x^*(t,f)$	$g(\nu,\tau)=g^*(\nu,\tau)$
P2	Time-frequency shift: $y(t)=x(t-t_0)\Rightarrow T_y(t,f)=T_x(t-t_0,f)$ $y(t)=x(t)e^{2\pi f_0 t}\Rightarrow T_y(t,f)=T_x(t,f-f_0)$	$g(\nu,\tau)$ independent of t and f

P3	Time marginal: $\int_{-\infty}^{+\infty} T_x(t,f)\,\mathrm{d}f = \left\|x(t)\right\|^2$	$g(\nu,0)=1 \quad \forall \nu$
P4	Frequency marginal: $\int_{-\infty}^{+\infty} T_x(t,f)\,\mathrm{d}t = \left\|X(f)\right\|^2$	$g(0,\tau)=1 \quad \forall \tau$
P5	Instantaneous frequency: $\frac{\int_{-\infty}^{+\infty} f T_x(t,f)\,df}{\int_{-\infty}^{+\infty} T_x(t,f)\,df} = -\frac{d}{dt}\left\{\arg\left(x(t)\right)\right\}$	$\left.\frac{\partial\left(g(\nu,\tau)\right)}{\partial\tau}\right\|_{\tau=0} = 0 \quad \forall \nu$
P6	Group delay: $\frac{\int_{-\infty}^{+\infty} t T_x(t,f)\,dt}{\int_{-\infty}^{+\infty} T_x(t,f)\,dt} = -\frac{d}{dt}\left\{\arg\left(X(f)\right)\right\}$	$\left.\frac{\partial\left(g(\nu,\tau)\right)}{\partial\nu}\right\|_{\nu=0} = 0 \quad \forall \tau$
P7	Finite time support: $x(t)=0$ if $\left\|t\right\| \geq T \Rightarrow$ $\Rightarrow T_x(t,f)=0$ per $\left\|t\right\| \geq T$	$\varphi(t,\tau)=0 \quad \left\|\tau\right\| < 2\left\|t\right\|$
P8	Finite frequency support: $X(f)=0$ if $\left\|f\right\| \geq B \Rightarrow$ $\Rightarrow T_x(t,f)=0$ if $\left\|f\right\| \geq B$	$\int_{-\infty}^{+\infty} g(\nu,\tau)e^{-j2\pi f\tau}\mathrm{d}\tau \quad \left\|\nu\right\| < 2\left\|f\right\|$
P9	Reduced interference	$g(\nu,\tau)$ is a low pass filter type in (ν,τ) plane

Table 3.1 - Properties of eight shift-invariant transforms and corresponding kernel conditions.

Transforms	**P0**	**P1**	**P2**	**P3**	**P4**	**P5**	**P6**	**P7**	**P8**	**P9**
Spectrogram (SPEC)	√	√	√							√
Wigner (WD)		√	√	√	√	√	√	√	√	
"Alias-Free" Wigner		√	√	√	√	√	√	√	√	
Pseudo-Wigner		√	√	√		√				
Smoothed-Pseudo-Wigner		√	√							√
Cone-Kernel		√	√					√		√
Reduced Interference		√	√	√	√	√	√	√	√	√
Choi-Williams (CWD)		√	√	√	√	√	√	√ **(*)**	√**(*)**	√

Table 3.2 - List of desirable properties satisfied by different quadratic transforms. (*) Not in a strict sense, but only approximately.

The WD does not satisfies P9 (reduced interference), which is a desirable property as it preserves only the authentic (e.g. modal) components. Detailed theoretical discussions on different TFRs may be found in the specialized literature [53,54].

3.1.4.5 Time-Frequency Representation of Stochastic Processes

3.1.4.5.1 Stationary processes

The notion of spectral density, which is well consolidated in the field of stationary processes, may constitute a valuable starting point for approaching non-stationary problems.

One of the reasons of the popularity of the Wigner transform is its desirable property to preserve the instantaneous spectral information in stationary processes. In fact, introducing the auto-covariance function of a process F, $C_F(t,\tau)=\mathrm{E}\{r_F(t,\tau)\}$, and taking the expectation in both sides of equation (3.33), we obtain the Wigner spectrum [11,19]:

$$\mathrm{E}\{WD_F(t,f)\}=\int_{-\infty}^{+\infty} C_F(t+\tau/2,t-\tau/2)\exp(-j2\pi f\tau)\mathrm{d}\tau \tag{3.37}$$

In the stationary case, the quantity expressed in equation (3.37) is independent of t and reduces to the usual spectral density: $\mathrm{E}\{WD_F(t,f)\}=S_F(f)$ [47,55]. In this situation, in fact, the covariance operator is a convolution operator, which is known to be diagonalized by the complex exponential functions.

Unfortunately, in practical applications a limited number of signals are available. If the process is ergodic, a WD estimate of the spectral density may be obtained from a single realization $x(t)$ by averaging over time instantaneous spectra [56]:

$$V_B(f)=\frac{1}{B}\int_{-B/2}^{B/2}\left|WD_X(t,f)\right|\mathrm{d}t \tag{3.38}$$

Based on equation (3.38) it also proves possible to quantify the degree of non-stationarity of a stochastic process on the given time interval via a distance measure [20]:

$$d_B{}^2(B,f)=\frac{1}{B}\int_{-B/2}^{B/2}\left|WD_x(t,f)\right|^2\mathrm{d}t-S^2{}_x(B,f) \tag{3.39}$$

If the process is stationary d_B reduces to zero. In multi-component signals, however, the Wigner representation of a single realization of the process is affected by interference terms, which can be filtered out in the ambiguity function domain but at the

cost of losing resolution. There is, in fact, a trade-off between cross term filtering and time-frequency resolution; hence the representation is kernel dependent. Another problem is that the Wigner transform misses the desirable property of non-negativity over the *t-f* plane [57]. These two aspects may have some negative implications in the definition of instantaneous estimators to be used in the analysis of deterministic signals.

Going back to linear TFRs, the square modulus of the STFT, or SPEC, of a stationary process may be written in the form [47]:

$$\mathrm{E}\left\{SPEC_F^{(\gamma)}(t,f)\right\} = \int_{-\infty}^{\infty} \left|\Gamma(f'-f)\right|^2 S_F(f)\,\mathrm{d}f' \tag{3.40}$$

where $\Gamma(f)$ is the spectrum of a window function $\gamma(t)$, such that $\left\|\Gamma(f)\right\|=1$, and $S_F(f)$ is the spectral density associated with the process. Equation (3.40) shows that the value of the spectrum at f is a weighted average of the spectral density, when $f \sim f'$. As long as the Fourier transform of the window is still localised near the origin, the spectrogram provides, for each fixed *f*, information on the part of the original signal which comes from the frequency contributions localised near f.

If one were to work with a sample realisation $x(t)$, by assuming the ergodicity of the signal, an estimator of the spectral density may be defined as follows [47]:

$$V_B(f) = \frac{1}{B}\int_{-B/2}^{B/2} SPEC_x^{(\gamma)}(t,f)\,\mathrm{d}t \tag{3.41}$$

Owing to the weighting average operation, the spectral function expressed by equation (3.41) is a biased estimator. A spectral function that supports a weighted average interpretation may be defined also for the SCAL [47].

3.1.4.5.2 Locally stationary processes

When a process is non-stationary, the covariance operator may have complicated time varying properties and its estimation is arduous because we do not know a priori how to diagonalize them. In the following we will focus on the particular class of locally stationary processes, i.e. processes whose covariance operators are approximately convolutions.

Recently, researchers have turned their attention to locally stationary processes as a tool to model systems where the behaviour varies as a function of time (e.g., Mallat et. al. [58], Dahlhaus [59], Ceravolo [60]). Though in the time-frequency plane the concept of local stationarity is easily grasped, to date it does not exist a universally accepted definition. In order to support an intuitive idea, suppose that for any t_0 the Wigner spectrum varies very little within an interval $[t_0-\delta, t_0+\delta]$. Such a parameter $\delta>0$ is called the stationarity length and in general its value depends on t_0.

The question on how to adapt the analysing window (or the kernel, in the case of a Cohen class transform) to the stationarity length of process is still open [47]. Several techniques have been formulated to select the best strategy and often they are based on optimisation procedures. For instance, Kozek [61] proposed a minimum bias optimisation criterion based on support properties of the ambiguity function. In principle, these methods are conceived to deal with stochastic processes or with a proper number of sample realizations and are not suitable to deal with a single signal.

Some new ideas may arise when working with random fluctuations produced by mechanical systems, which typically change slowly in time or space. This type of signals can be generally considered as locally stationary, since they appear in the time-frequency plane as a sum of modulated harmonics concentrated at the modal frequencies. In this case, the instantaneous spectrum of a single realization may reflect and be associated with some physical parameters, whose consistency is an indirect indicator of the transform suitability.

A simple case of locally stationary process is a uniformly modulated process that is constructed as $x(t)=c(t)x_0(t)$, where $c(t)$ is a slowly varying modulation function and $x_0(t)$ some stationary process. The time evolutions of such a process are depicted correctly by the following time-varying spectrum [62]:

$$P_F(t,f)=c^2(t)S_{F_0}(f) \tag{3.42}$$

When dealing with more general classes of oscillatory processes, a description of temporal evolutions of spectral components, frequency by frequency, produces:

$$x(t)=\int_{-\infty}^{+\infty} A_x(t,f)X(f)\mathrm{e}^{\mathrm{j}2\pi ft}\mathrm{d}f \tag{3.43}$$

thus leading to Priestley's evolutionary spectrum [25,26]:

$$P_F(t,f)=\left|A_F(t,f)\right|^2 S_F(f) \tag{3.44}$$

The modulation function $A_F(t,f)$ is supposed to undergo a slow time evolution, which ensures an almost orthogonal decomposition. Priestley's spectrum retains satisfactory properties (e.g. non-negativity) but misses uniqueness.

In locally stationary conditions, evolutionary representation supports an interesting time-frequency input-output relationship [63]:

$$y(t)=\int_{-\infty}^{+\infty} H(t,f)A_x(t,f)X(f)e^{j2\pi ft}\mathrm{d}f \tag{3.45}$$

where $H(t,f)$ is the transfer function of a time varying filter. The important result is that the output is a modulated form of the filter (or system) transfer function. This is analogous to one-dimensional filtering in the frequency domain: $Y(f)=H(f)X(f)$.

Finally, it is worthwhile noting that there is a theoretical link between evolutionary spectra and members of Cohen class of transforms [64] and, what is more, for slowly varying processes the Wigner spectrum approaches the evolutionary spectrum.

3.1.4.6 Time-Frequency estimation and best windowing

An attractive idea is to extend by analogy some properties of stationarity to local stationarity. For instance, an estimator for the time-varying spectrum of a locally stationary process, $T_F(t,f)$ may be obtained from a single realization $x(t)$ by selecting a proper analysis window/kernel and posing $B=\delta$ in equations (3.38) and (3.41):

$$V_F(t,f)=\left|T_x(t,f)\right| \tag{3.46}$$

where $T_x(t,f)$ is any quadratic TFR. It is likewise possible to track instantaneous relationships between signals. For instance, in multi-channel measurements on structures, instantaneous estimators of amplitude ratio and phase difference between channels may be defined as follows [65,66]:

$$AR_{ij}(t,f)=\sqrt{\frac{T_{x_i}(t,f)}{T_{x_j}(t,f)}}\ ;\ PH_{ij}(t,f)=phase\left\{T_{x_i,x_j}(t,f)\right\} \tag{3.47}$$

In linear time-invariant systems, equation (3.47) can support output-only modal identification procedures, as stability over time of such estimators discriminates modal components from exogenous frequency components. In fact, modal signals are characterised by amplitude and phase relationships that are not time-dependent and therefore their modal shape is constant over time. The identification of modal frequencies therefore reduces to a search for the particular values $f=f_k$ for which the estimators remain constant with respect to the time variable, in general by resorting to multiple criteria techniques. In frequency intervals where a single modal component is predominant, the estimators tend to lead to a constant value in time. This property is progressively closer satisfied up to an actual constant value at the modal frequencies.

Modal frequencies may be identified as minima in standard deviation plots defined as:

$$\int_0^T\left[PH_{ij}(t,f)-\overline{PH}\right]^2\mathrm{d}t \tag{3.48}$$

where T is the length of the analysed signal and $\overline{PH}$ indicate the mean value.

Once the modal frequencies have been identified, equations 33 supply the temporal evolution of the amplitude and phase ratios. Alternatively, modal shape estimators can be taken as:

$$AR_{ij}(t,f)\Big|_{f=f_k} = \left|\frac{T_{x_i z^{(k)}}(t,f)}{T_{x_j z^{(k)}}(t,f)}\right|_{f=f_k} \quad PH_{ij}(t,f)\Big|_{f=f_k} = phase\left\{\frac{T_{x_i z^{(\omega)}}(t,f)}{T_{x_j z^{(\omega)}}(t,f)}\right\}\Bigg|_{f=f_k} \tag{3.49}$$

where $z^{(k)}(t)$ is a signal generated as a sinusoid with frequency equal to the k^{th} modal frequency. The procedure is then repeated for all the signals at the i^{th} and j^{th} position. Recently an improvement of this technique, based on the principal component analysis, was proposed [67].

3.1.4.6.1 Best windowing

Typical questions about time-frequency estimation are how to select the optimal representation and window analysis and how many realizations of the process are needed to obtain an accurate estimate for $T_F(t,f)$.

While quadratic representations are very useful in analysing strongly non-stationary signals, choosing the best kernel for a particular application appears to be a challenging task, as relationships with dynamic response characteristics are far from being trivial.

An alternative idea may consist in being satisfied with linear representations, which lend themselves to a clearer interpretation, and accepting the errors due to the fact that linear TFRs cause in general a distortion in the representation of the instantaneous power of stationary stochastic processes.

In principle, a suitable choice for the window of a STFT should be a function compactly supported in the interval $[t_0-\delta, t_0+\delta]$, and may vary according to a temporal law matched to the stationarity length of the process. Unfortunately, in most practical applications the stationarity length δ is unknown.

Numerical studies have been performed in order to identify the influence of the analysis window on instantaneous spectral estimation via a STFT spectral function (equation (3.41)). To this aim, an extensive set of dynamic response signals has been created numerically by exciting simple linear oscillators by means of white noise. The results reported here will focus on the following factors: type of window, window length (in samples), decorrelation length of the process (related to damping) [43].

Equation (3.40) shows that the window may cause an error in the estimate and that the latter, when the number of realizations approaches infinity, decreases with increasing window temporal length. The effect of the window length as well as the type of window has been examined by Ceravolo [43].

The results, shown in Figure 3.2a, indicate that, averaging over a finite number of realizations (in this case 30 demonstrated to be sufficient for a virtually exact fitting), windows of optimal length exist for the estimate of the "frequency response function"

(FRF) and hence for the identification of modal parameters via linear TFRs. Such lengths are identified by minimum points in charts of the type shown in Figure 3.2a.

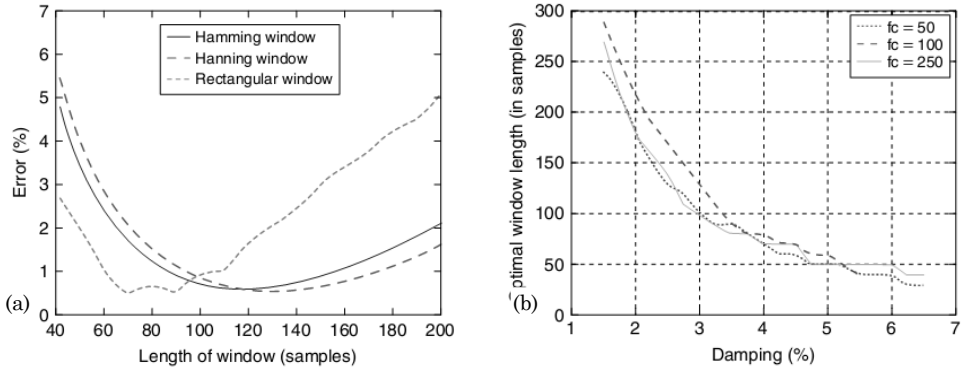

Figure 3.2 - (a) Error in the curve fitting performed on STFT as a function of window length (average over 30 realizations). (b) Optimal length in samples of the STFT (Hanning window) as a function of system's damping: curves obtained for three different values of sampling frequency.

In stationary conditions, the parameter that may affect the quality of time-frequency representation demonstrated to be the decorrelation length, and hence damping, whilst other factors such as the window shape were seen to be less relevant, at least for typical analysis windows [43]. Figure 3.2b, which has been obtained from simulated examples, shows the evolution of the optimal length that the windows should have as a function of damping level (in this case for a Hanning type window). This type of chart may be of practical use when representing the response of structures under ambient excitation. The choice of the optimal length for the STFT analysing window, based on Figure 3.2b, is conditioned by the availability of a raw estimate of damping.

3.1.4.7 Model based Time-Frequency estimation

While linear representations, which permit a filter-bank interpretation, clearly allow reconstruction of the signal (e.g. equation (3.16)), for energy decompositions the same property is less obvious. For Cohen class of transforms the inversion is obtained from [68]:

$$x(t')^{*}\,x(t)=\int_{-\infty}^{+\infty}\int_{-\infty}^{+\infty}\int_{-\infty}^{+\infty}\frac{T_x(u,f)}{g(\nu,t-t')}e^{j2\pi f(t-t')+j2\pi\nu\left[u-(t-t')/2\right]}\mathrm{d}u\mathrm{d}f\mathrm{d}\nu \tag{3.50}$$

By taking a particular value of *t'*, for instance zero, we have:

$$x(t)=\frac{1}{x(0)^{*}}\int_{-\infty}^{+\infty}\int_{-\infty}^{+\infty}\int_{-\infty}^{+\infty}\frac{T_x(u,f)}{g(\nu,t-t')}e^{j2\pi ft+j2\pi\nu(u-t/2)}\mathrm{d}u\mathrm{d}f\mathrm{d}\nu \tag{3.51}$$

One can easily notice that, according to equation (3.50), the signal can be recovered but only to within a constant phase factor.

3.1.4.7.1 Signal synthesis

In many practical applications, e.g. earthquake accelerogram generation, the main interest is in synthesizing signals with specific time-frequency features, rather than in signal reconstruction. Synthesis algorithms can also be used to perform time-varying filtering, multi-component signal separation, and window and filter design. In this perspective, one might envisage filtering in the *t-f* plane with [54,69]:

$$\tilde{T}(t,f) = \Gamma(t,f)T(t,f) \tag{3.52}$$

where $\Gamma(t,f)$ is referred to as time-frequency mask.

A major problem of the masking approach is that not all two dimensional functions are valid TFRs. Instead, it is natural to resort to optimization techniques (e.g. least square methods), in order to find a time-frequency decomposition that best fits a time-frequency model.

Synthesis algorithms are usually formulated to find a signal $x(t)$ that minimises the error ε_x between a given model, $\tilde{T}(t,f)$, and the transform of the signal $T_x(t,f)$ to be synthesized [41,54,69]:

$$\varepsilon_x = \left\| T_x(t,f) - \tilde{T}(t,f) \right\| \longrightarrow \min_x \tag{3.53}$$

Since for WD and other shift-invariant transforms the solution of the optimization process is not unique (e.g. $x(t)$ and $x(t)e^{j\alpha}$ have the same Wigner representation) the algorithm often contains a step to find the optimum phase factor.

Under particular conditions it proves advantageous to represent $x(t)$ in an ortho-normal basis. Thus, by assuming a quadratic TFR, equation (3.53) becomes:

$$x(t) = \sum_k \alpha_k q_k(t), \quad \varepsilon_x = \left\| \sum_k \sum_l \alpha_k \alpha_l^* T_{kl}(t,f) - \tilde{T}(t,f) \right\| \longrightarrow \min_\alpha \tag{3.54}$$

such a formulation is certainly valid for linear dynamic systems, whose response is a sum of modal components.

3.1.4.7.2 Model identification

A formulation similar to that of equation (3.52) may be used also in solving the inverse problem, namely finding a model that produces the same distribution as a measured signal.

When $x(t)$ is measured on a linear structure and we want to identify the dynamic model, a modal decomposition form is indicated for $\tilde{T}(t,f)$. As an example, a model identification can be obtained from the following unconstrained minimization [60]:

$$\varepsilon_x = \left\| \sum_k \sum_l \alpha_k \alpha_l^* \tilde{T}_{kl}(t,f) - T_x(t,f) \right\| \longrightarrow \min_{\mathbf{p}} \tag{3.55}$$

where **p** is the global vector of parameters, which may contain α terms as well as other parameters of the model.

In some applications, as in structural control, the optimization can be performed on an on-line basis. For instance, a "block-by-block" synthesis/identification algorithm is performed on local, finite record intervals, whose length will depend necessarily on the time-frequency analysis window or kernel. When parameters to be estimated retain a temporal significance (e.g. time-varying systems [70] or output-only identification) it may prove advantageous to perform an instantaneous minimization so as to obtain a punctual estimate of **p**:

$$\varepsilon_x(t) = \left| \int_{-\infty}^{+\infty} \left[\tilde{T}(t,f) - T_x(t,f) \right] df \right| \longrightarrow \min_{\mathbf{p}} \tag{3.56}$$

The most convenient minimisation form and algorithm will depend on the specific application. In the implementation of equations (3.52)-(3.55), the analytic signal is usually preferred to the real one, since it avoids cross-term interference between positive and negative frequencies.

3.1.4.7.3 Output-only identification of linear systems

Natural excitation of flexible structures (buildings, bridges, antennas etc.) is characterized by slow energy supply. Also based on the time-varying filter interpretation evoked in equation (3.45), in the time-frequency representation of locally stationary signals we expect energy to concentrate around modal frequencies and be modulated according to the evolution of the TFR of the modulating waveform [43,50]. Consequently, the time-frequency model in equation (3.55) may be given the following (non-negative) form [43]:

$$\tilde{T}(t,f) = \sum_k \sum_l \alpha_k(t) \alpha_l^*(t) \tilde{H}_k(f) \tilde{H}_l^*(f) \tag{3.57}$$

where $\tilde{H}_k(f)$ is a scaled version the k-th mode's FRF. In particular, for viscously damped dynamic systems the following expression holds:

$$\tilde{H}_k(f) = \left(f_k{}^2 + 2j\zeta_k f f_k - f^2 \right)^{-1} \tag{3.58}$$

If the assigned TFR has a stochastic nature (possibly obtained by ensemble averaging) and its modal components are uncorrelated, the cross-terms vanish from equations (3.54)-(3.55). Correspondingly also $T_F(t, f)$ will tend to non-negativity in accordance with the model in equation (3.56).

It is noteworthy that interference term suppression, as operated on deterministic signals by specific TFRs (property P9 in table 3.2), appears to produce in equations (3.54)-(3.55) effects that are similar to those produced by a stochastic identification.

3.2 Assimilating experimental results in numerical models (model updating)

There are two main complementary approaches to the calibration of a model: a *model-driven* and a *data-driven* approach. Also the nature of the problem changes depending on the type of approach which is pursued.

In the case of the model-driven methods the parameters of the model (or at least part of them) are unknown and must be obtained from the measured data. In this case a version of the model is constructed using physical laws based on first principles. Then the model parameters are changed by means of some optimisation techniques to fit the measured data. This procedure is commonly known with the name of Model Updating (MU).

The data-driven approach consists in a forward evaluation problem and it is treated as a *Statistical Pattern Recognition* (SPR) problem. In its broader sense pattern recognition consists in the labelling of a sample of measured data according to a series of pre-defined classes. Pattern recognition finds applications in several engineering, economic and social fields.

3.2.1 Model-driven approaches

Model updating is a technique that has been developing through the last years. In various fields of the engineering the usage of numerical models to evaluate the behaviour of a physical system is frequent. The accurate representation of a system depends of the type of numerical model used to represent the elements of the system and on the properties of this model (e.g. in a structural application the elasticity modulus, boundary conditions, et cetera). The discrepancies between the behaviour of a numerical model and the real system can be significant as reported by [71] and [72].

Inverse methods are commonly used to improve the quality and reliability of a model. They combine an initial (generally finite element) model of the structure, whose parameters can be derived by specific characterisation tests or simply guessed, and measured data expressed in the form of modal properties or frequency response function.

In the comparison between analytic data and experimental data there is a potential problem: the response is measured only in a limited number of points of the

structure, and in a limited interval of frequencies. Therefore, to compare these different set of data is necessary to expand the measured data or to reduce the analytic data.

3.2.1.1 Modal reduction

There are different types of modal reduction. The so-called static reduction or Guyan's reduction [73] allows calculating a transformation matrix T which reduces the mass and the stiffness matrices to the terms related to the useful degrees of freedom.

The dynamic reduction is an extension of the Guyan's method, accounting of the inertial terms for a particular frequency. In this case is possible to reach higher precision respect to the static reduction [74].

An Improved reduction system (IRS) has been introduced by O'Callahan [75]which improves the static reduction method through the introduction of inertial terms as pseudo-static forces.

O'Callahan and others have developed also the System Equivalent Reduction Expansion Process (SEREP) which utilizes the computation of eigenvectors to produce the transformation between master and slave coordinates [76].

3.2.1.2 Modal expansion

Modal expansion is a procedure strictly related to modal reduction, and is possible to look at it as an inverse reduction.

The easier way to expand data is to substitute the unknown eigenvector values with the values calculated from the analytical model but using this procedure both analytical and measured modal shapes have to be normalized in the same way.

It is possible to expand data using the stiffness and mass matrices. This procedure is dual to the dynamic reduction [74].

An alternative method is to use modal data coming from the finite element analysis. The identified modes are treated as a linear combination of the analytical modes and in this way it is possible to calculate a transformation matrix. This procedure is strictly linked to the previously mentioned SEREP procedure.

3.2.2 Direct methods and sensitivity analysis

Model updating methods may be classified as direct or sensitivity methods. Direct methods try to reproduce the measured data from the structure by applying little changes to the stiffness and mass matrix which are difficultly associable to the parameters of the model. Indeed, the main drawback of direct methods is that their results are characterised by a lack in the physical meaningfulness. More details about these methods can be found in [77,78,79,80,81,82,83].

Sensitivity-based methods are more widespread with comparison to direct methods because of their capability to calibrate the model taking the influence of the updating parameters of the different structural elements into account. They offer a wide range of parameters to update that have physical meaning and allow a degree of control over the optimization process. All these parametric methods rely on the definition of a so-called "penalty function" which is computed as the quadratic norm of the differences

between the measured and the numerical quantities. The discrimination among the methods is based on the choice and the number of parameters to compute the objective function and the optimisation technique used to minimise it. Recently heuristic techniques like Simulated Annealing [84,85], Genetic Algorithms [86] and Evolutionary Strategies [87] and probabilistic approaches have supplanted traditional methods to solve non-linear problems like Newton-Raphson. New developments in optimisation techniques consent different approaches to the problem, such an optimisation through all the Pareto set of solution, performing a multi-objective minimization [88].

3.2.3 Parameterisation of the model

The choice of the structural parameters that have to be updated is influenced on the typology of the modelled structure and on the uncertainty level which affects the model. Once the model is defined the most important task in a model updating procedure is the choice of the parameter to update. The sensibility to a single generic parameter θ, according to Wittrick [89] and Fox-Kapoor [90] is given by:

$$\left[\mathbf{K}-\lambda_j\cdot\mathbf{M}\right]\cdot\frac{\partial\{\Phi\}_j}{\partial\theta}=-\left[\frac{\partial\mathbf{K}}{\partial\theta}-\lambda_j\frac{\partial\mathbf{M}}{\partial\theta}-\frac{\partial\lambda_j}{\partial\theta}\cdot\mathbf{M}\right]\cdot\{\Phi\}_j \tag{3.59}$$

It is possible to rearrange this formula in order to calculate the sensibility of the single eigenvector. In particular types of problems it may be useful to calibrate different part of the model. Generally, several elements sharing the same properties are merged into a single macro-element in order to reduce the number of parameters to update and to ease the research of the optimal solution. In this case is possible to update single parts of the stiffness and mass matrices:

$$\mathbf{M}=\mathbf{M}_0+\sum_{i=1}^{n}\theta_i\cdot\mathbf{M}_i \tag{3.60}$$

$$\mathbf{K}=\mathbf{K}_0+\sum_{i=1}^{n}\theta_i\cdot\mathbf{K}_i \tag{3.61}$$

where [M] and [K] are the global matrices and $[M]_i$ and $[K]_i$ are the matrices of the group of elements that needs update.

In the case that the parameter θ assumes the aspect of a physical quantity as the elastic modulus, the volumetric mass or the Poisson's modulus is impossible to apply (8) and (9), because the linearity between parameter and matrices is not guaranteed anymore. The Young's modulus and the moment of inertia of the most uncertain elements are usually considered because they are directly related to the stiffness of the elements. In this case is possible to expand in Taylor series obtaining:

$$\mathbf{M} = \mathbf{M}_0 + \sum_{j=1}^{n} \frac{\partial \mathbf{M}}{\partial \theta_j} \cdot d\theta_j \tag{3.62}$$

$$\mathbf{K} = \mathbf{K}_0 + \sum_{j=1}^{n} \frac{\partial \mathbf{K}}{\partial \theta_j} \cdot d\theta_j \tag{3.63}$$

3.2.4 Comparison between identified and analytical data: MAC and COMAC

The measurement data used to compute the objective function may belong to the frequency or modal domain. Time domain data are generally disregarded because measured time-series are affected by noise and their volume of data is difficult to handle. Data compression is performed to obtain FRF data, which are less affected by random noise because averaged but suffer little loss of information in the passage from time to frequency domain. Model updating methods based on modal parameters like natural frequencies, mode shapes and damping ratios exploit a further reduction in the number of data points but they have to cope with the reduction of accuracy in the modal parameters estimation. Furthermore, mode shapes are valuable parameters to be implemented in a model updating procedure because they allow pairing the analytical and experimental modes but their precise estimation is difficult to reach and changes due to damage are often smaller than the error bounds on corresponding measurements. In literature is possible to find many functional indexes that consent to compare measured and numerical data. Among the most used there is the MAC (Modal Assurance Criterion), defined as:

$$MAC_{jk} = \frac{\left(\{\Phi_m\}_j^T \cdot \{\Phi_a\}_k \right)^2}{\left(\{\Phi_a\}_k^T \cdot \{\Phi_a\}_k \right) \cdot \left(\{\Phi_m\}_j^T \cdot \{\Phi_m\}_j \right)} \tag{3.64}$$

where $\{\Phi_a\}_k$ is the theoretical eigenvalue corresponding to the k^{th} mode, and Φ_{mj} is the measured eigenvalue, corresponding to the j^{th} mode. The MAC can vary between 0 and 1, and the comparison could be considered satisfied with a MAC value superior to 0.8.

The COMAC (Co-ordinate MAC) quantifies the correlation between identified and analytical modal shapes referring to a particular degree of freedom:

$$COMAC(j) = \frac{\sum_{i=1}^{N} \{\Phi_a\}_{ji}^T \cdot \{\Phi_m\}_{ji}}{\left(\sum_{i=1}^{N} \{\Phi_a\}_{ji}^2 \right) \cdot \left(\sum_{i=1}^{N} \{\Phi_m\}_{ji}^2 \right)} \tag{3.65}$$

where i is the ith modal shape and j is the jth degree of freedom.

Many authors use a Weighted MAC (WMAC) which utilises a weight matrix. The weights can depend from the reliability of certain data (due to the distribution or the accuracy of the sensors). Among the others, it is also possible to remind:

- Partial Modal Assurance Criterion (PMAC);
- Modal Assurance Criterion Square Root (MACSR);
- Scaled Modal Assurance Criterion (SMAC);
- Modal Assurance Criterion using Reciprocal Vectors (MACRV);
- Modal Assurance Criterion with Frequency scales (FMAC);
- The Enhanced Coordinate Modal Assurance Criterion (ECOMAC);
- Inverse Modal Assurance Criterion (IMAC);

For a review of all these MAC-derived criteria and a complete bibliography, consult [91].

Another approach is to compare, instead of the modal shapes, the frequency response functions, with the same principle of the MAC. This comparison is feasible in the case of experimental tests performed with a vibrodyna. In this case it is called Frequency Response Assurance Criterion (FRAC). The Complex Correlation Coefficient (CCF) and the Frequency Domain Assurance Criterion (FDAC) derive from the previous.

3.2.5 Data-driven approaches

Differently from the model-driven methods, in the forward approach the knowledge of the phenomena ruling the structural behaviour is not derived from physical laws implemented in a model but is extracted directly from the data or based on a priori information, if available. The PR algorithm is trained to recognise the correspondence between samples of data and type classes [92]. Two different types of learning do exist. In the *supervised learning* several sets of training data are presented along with the corresponding class they belong to. Both the uniqueness of the correspondence between a set of measurements and its class and the exhaustiveness in the presentation of all the possible classes are fundamental requirements. The availability of patterns concerning the state of the structure represents the major obstacle for this type of learning. *Unsupervised learning* does not require prior information about the state of the structure; only data from the normal operating condition of the structure are needed to create a model of normal condition which is compared with all the new acquired data samples to detect changes. Two sources of data can be exploited: numerical modelling or experiment. The former presents the same drawbacks of the inverse problem approach. They are related to the dependence on a model of the structure whose properties may be uncertain, the constitutive laws of the materials not accurately defined and the analyses excessively time-consuming. On the other hand, the collection of training sets from experiments is even harder to accomplish because it requires several replica of the same system according all the possible scenarios which might affect the structure [93,94].

3.2.6 Perspectives and remarks

The calibration of numerical models, through experimental data, has been a ground-breaking advancement in the field of numerical simulation. The advantage of distributed model in producing distributed predictions provided by updating is in contrast

with traditional experimental testing, which allowed to characterise the model of a structure only locally. A need exist for the use of confidence levels which may be assigned to quantified mesh, or test data, uncertainties.

In the field of model updating one of the main research branch nowadays is the stochastic model updating, which may compensate in some way a possible lack of data [95,96]. This type of approach provides a suitable safeguard against severe underestimation of the variability of the parameters derived from a small sample set.

3.2.7 Stochastic model updating

The usual model updating methods may be considered to be deterministic since they use measurements from a single test system to correct a nominal finite element model. Anyway, there may be variability in virtually identic test structures and uncertainties in the FE model [93]. This variability in the test structures may arise from many sources including geometric tolerances and the manufacturing process, and modelling uncertainties may result from the use of nominal material properties, ill-defined joint stiffness's and rigid boundary conditions.

The choice of updating parameters is an important aspect of the process and should always be justified physically. Model uncertainties should be located and parameterised sensitively to the predictions. Finally, the model should be validated by assessing the model quality within its range of operation and its robustness to modifications in the loading configuration, design changes, coupled structure analysis and different boundary conditions. But predictions based on a single calibration of the model parameters cannot give a measure of confidence in the capability of numerical simulations to represent the actual structure. The credibility of the structural model must combine three components:

- an assessment of the fidelity of predictions to test data;
- an assessment of robustness to variability, uncertainty and lack of knowledge;
- an assessment of prediction accuracy in situations in which the test measurements are not available.

The three goals of fidelity-to-data, robustness-to-uncertainty, and confidence-in-prediction are antagonistic and a trade-off has to be achieved.

The parameter estimation problem can be presented within a statistical/probabilistic framework basically in two different ways corresponding to the frequency interpretation of probability or the degree of belief interpretation. The maximum likelihood (or maximum log likelihood) approach consists of determining the maximum of the conditional probability of the parameters on the basis of known random output measurements; this is a frequency approach. Bayesian methods, on the other hand require an additional input not needed by the maximum likelihood method, a prior probability distribution for the parameters, which embodies our judgement of how plausible it is that the parameters should have certain values. The selection of the priors is an extremely controversial aspect of the method since it is a subjective, degree of belief, judgement.

Amongst the earliest papers dealing with finite element model updating, the seminal work by Collins *et al* [97] adopted a linearized sensitivity approach with the statistics of the unknown parameters determined from vibration measurements with

random errors. The approach, a "best linear unbiased estimator", can be considered equivalent to a weighted least-squares method with the weighting matrix given by the inverse data covariance matrix. More recently, Beck and his colleagues [98,99] developed a model updating approach using Bayesian inference. As with the work of Collins *et al* [97] the statistics of the uncertain finite element parameters are determined on the basis of randomness in the measurements from a single test piece, i.e. randomness due to manufacturing and material variability in a number of nominally identical test structures is not considered. In fact, this latter variability is very much more significant than measurement noise.

The treatment of uncertainty and quantification of errors is in general a two-step process, the first step being the identification of all uncertainty and error sources whether they originate from the modelling assumptions, numerical computations or physical experiments. The second step is the assessment and propagation of the most significant uncertainties and errors through the modelling and simulation process to obtain the predicted response quantities. Neal [100] discusses the Markov Chain Monte-Carlo method, used for the solution of integrals arising in Bayesian inference and having applications including neural networks and simulated annealing.

Multiple realisations of an experiment (numerical or physical) lead to the concept of the meta-model [101] and the possibility to express the distance between models and operate design modifications based on statistical concepts as opposed to the comparison between deterministic models based on nominal variables. As a result of Monte-Carlo simulation, the meta-model represents a source for a statistical problem description, confidence measures, correlation with experimental data, global dependencies and selection of dominant design variables. For instance, Fonseca *et al* [102] used a maximum likelihood method to solve the inverse problem of a cantilever with a lumped mass at an uncertain position.

In the preceding discussion, randomness is confined to discrete parameters whereas in practice it may be distributed over areas or volumes, such as in the case of uncertainty in the thickness of a plate dependent upon spatial coordinate, and should therefore be properly represented by a random field. For what concerns this aspect of the problem, generally referred as spectral stochastic finite element method (SSFEM) one can read Ghanem and Spanos [103]. Ghanem and Red-Horse [104] carried out a vibration analysis of a space-frame with joints having distributed random material properties. All uncertainty propagation techniques rely on large amounts of computation. The SSFEM is particularly demanding computationally.

3.3 Examples of experimental modal analysis of masonry structures

3.3.1 Experimental modal analysis in buildings

As previously stated, the modal analysis is the process of determining the inherent dynamic characteristics of a system in forms of natural frequencies, damping factors and mode shapes, and using them to formulate a mathematical model for its

dynamic behaviour. The formulated mathematical model is referred to as the modal model of the system and the information for the characteristics is known as its modal data.

The execution of the experimental tests and the analysis of the measurements have to be defined accordingly to the type of structure under exam and to the characteristics that need to be determined. The excitation source can be known, by using a force to excite the system, but more often it can be used the environmental noise (such as wind or traffic). In the latter case the excitation results unknown. This type of excitation presents several advantages with respect to forced excitation: there is no need to apply external loads and external special devices and, more important, there is no need to measure the excitation (which can be tricky sometimes). With no need to apply external loads there are no risks to damage the integrity of the structure, which can be a limiting factor in the case of architectural heritage structures. Moreover, environmental excitation virtually allows acquiring an unlimited set of data because the input source is always present. This feature is exploited particularly in structural health monitoring systems, in order to monitor continuously the dynamic parameters of the structure.

The linear identification techniques used are the so-called output only methods which usually work in the time domain. In this framework it is useful to distinguish among non-parametric and parametric identification methods.

The linear identification techniques used are the so-called output only methods which usually work in the time domain. The results of the identification achieved using these techniques may be unreliable due to the presence of a source of excitation which cannot be assumed to be white Gaussian noise or to a random stationary signal. In other cases the excitation can be so weak that is not able to excite all the needed modes. A non-stationary input, together with noise in the measurement of data leads to limitation in the applicability of the aforementioned techniques, because in such a case the structural response cannot be considered time-invariant anymore. This limitation can be overcome by using convenient windowing techniques of the signals, in order to individuate part of the response which can be still considered stationary.

Table 3.3 shows a summary of the principal linear identification methods that have been successfully applied in the experimental modal analysis of masonry structures.

Domain	**Excitation**	**Methods**
Time	Known	Ibrahim Time Domain (ITD) [16] Auto-Regressive Moving Average (ARMA)
	Unknown	Eigenvalue Realization Algorithm (ERA) [17] Stochastic Subspace Identification (SSI) [12] PolyReference Time Domain (PRTD) [20] Second Order Blind Identification (SOBI) [105]
Frequency	Known	Rational Fractional Polynomial (RFP) [31] Goyder method [34]
	Unknown	Spectral Analysis [106] Frequency Domain Decomposition (FDD) [40]
Time-Frequency	Known	Time-Frequency Instantaneous Estimators (TFIE) [65,107]

Table 3.3 - Principal linear identification methods used in the identification of masonry structures.

3.3.2 SS. Annunziata Bell-Tower in Roccaverano

The first case study reported is the SS. Annunziata church bell-tower in Roccaverano. A vibration test campaign was carried out on a XVI century church bell-tower rising in Roccaverano (Asti-Italy) whose style inspired by the school of Bramante (Figure 3.3). In the past the church was exposed to a strong earthquake which caused serious damage both on the facade and on the bells-tower and subsequently some interventions of restoration were made. The tower has been subjected to an extensive experimental investigation both under ambient vibrations and actions induced by the bells.

Vibration measurements were performed on the bell tower only, by placing the accelerometers on the landings, arranged in the horizontal direction. Each set-up is made up of the signals relating to four acquisition channels, of which two were fixed as reference channels and two were moved to the levels of the different landings. The measurements were made separately in the E-W and N-S directions, but one of the tests was conducted with two accelerometers arranged in the orthogonal direction, according to the two main axes of the bell tower, in a central position. This made it possible to correlate the modal shapes observed in the two main directions and to build up space modal shapes, of special importance in connection with torsional modes.

Different types of excitation were used, and namely, the one generated by bell tolling in two different directions, the one produced by pulses applied to the bells and finally the one arising from environmental noise. An aspect to be noted is the absolute absence on Fourier spectra of important components in the 2.5-10 Hz range, namely a frequency range within which the second flexural mode and the first two torsional modes are typically located in structures of this type.

Let us now examine the results obtained with the TFIE method. For the sake of brevity, in lieu of the two-dimensional estimator, we give the charts of the standard deviation of the estimator as a function of frequency, as this makes it possible to identify each modal frequency as a relative minimum in scatter due to the constancy of modal amplitude ratios or phase differences. In the following we shall refer to the phase estimators, which admit a much clearer interpretation than the amplitude ones. Figure 2 shows a sample phase difference estimator; this kind of diagram displays very clear minimum points and it also identify frequencies which did not appear at all in the PSD's. The results are listed in table 3.4.

It was clearly observed the existence of a first predominant mode in the N-S direction, i.e. at 1.66 Hz according to the less stiff direction, and another prevalent mode in the E-W at 2.26 Hz. These modes, which were also quite evident in Fourier spectra, were then immediately associated with the first two flexural modes according to the two main axes. The mode at 4.67 Hz (Figure 3.5), observed in either direction, was associated with a first torsional mode.

All in all, the results of the identification process based on the time-frequency estimators offer information which is totally new with respect to the peaks observed in energy spectra. This prompted the need to construct a simplified and yet reliable FE model to work out a correct classification of the modes [66].

Figure 3.3 - SS. Annunziata church and bell-tower in Roccaverano (Asti), Italy.

The following data were used to build up a simplified truss model of the bell-tower:

1) The geometric data of the structure;

2) Frequencies for which solid identification and physical evidence had been collected: 1.66 Hz, first flexural mode in the N-S and 2.26 Hz direction, first flexural mode in the E-W direction.

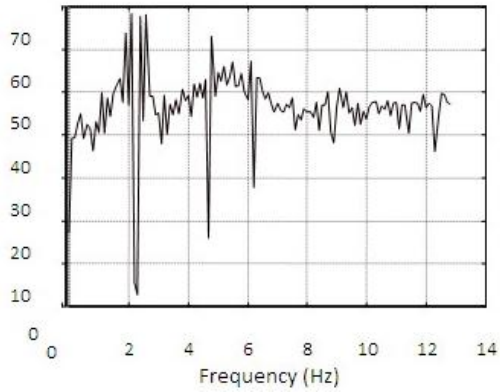

Figure 3.4 - SS. Annunziata bell-tower: standard deviation of sample phase difference estimator as a function of frequency.

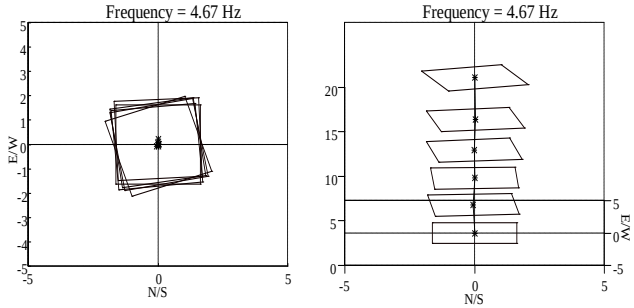

Figure 3.5 - SS. Annunziata bell tower: a sample mode identified in the range 1-5 Hz (1st torsional).

Mode	Identified frequencies (Hz)
1	1.66
2	2.26
3	4.67
4	6.18
5	6.40
6	8.90

Table 3.4 - SS. Annunziata bell tower: first six modal frequencies as identified through TFIE method

The chosen model was a space truss (Figure 3.6), whose horizontal members represent the flexural stiffness of the bell tower and the diagonals simulate the shear stiffness of the masonry panels. Albeit approximate, this model makes it possible to exploit the geometric data available in the determination of stiffness values, thereby reducing the number of parameters to be calibrated to the elastic properties of the material.

The geometric data were exploited according to the following criteria:

- the plan dimensions of the model reflect the distances between the outer walls;
- the uprights of the lattice, which are assigned a very high stiffness value, are situated at the landings, where the accelerometers were placed;
- from a careful examination of the vertical sections of the bell tower and the preliminary modal shapes observed, it can be seen that over a certain height, of ca 3.5 m, the bell tower constitutes a single body with the church building;
- additional constraints were introduced in the form of 4 horizontal struts placed at the level of the first landing, to represent the influence of the church;
- the areas of the vertical members of the lattice were determined so that, at each level, the moments of inertia of the lattice along the two main axes would equate the moment of inertia of the structure. The elasticity modulus (E) was assumed to be uniform over the entire tower;
- the stiffness of the diagonals was determined so as to equate the shear stiffness of the panels. The area of the panels was known, whilst the tangential elastic modulus (G) remained unknown. For the two storeys having no openings, a fictitious modulus (G^*), which cannot be directly correlated with the material properties, was considered.

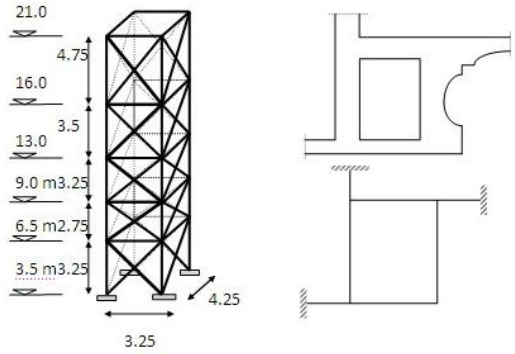

Figure 3.6 - SS. Annunziata bell tower: simplified truss model.

The unknowns of the calibration process boiled down to five: the E and G moduli, the fictitious modulus G^* and the stiffness parameters, k_1 and k_2, of the struts simulating the restraint.

The calibration process, conducted by means of an iterative procedure, consisted of minimizing a cost function:

$$E = \sum_{i=1}^{n} \left(\frac{f_{mi} - f_{ci}}{f_{ci}} \right)^2 \tag{3.66}$$

where f_{ci} are the frequencies calculated through the calibration process, and f_{mi} are the measured frequencies. It should be noted that, in addition to making the calibration process more significant, the use of a physical model related to the geometric data actually measured also reduces the risk of dealing with an ill-conditioned problem.

A first test was conducted by including in the cost function only the first two frequencies, namely the first flexural frequencies along the two principal axes, which are the most accurate and reliable one. After checking the reliability of the modes identified this far, a new calibration process was performed to include the fourth frequency, i.e. the second flexural frequency in the N-S direction. The quality of the results was significantly improved. Table 3.5 provides an overview of the frequencies of interest supplied by the calibrated model.

The values taken on by the parameters after the calibration process are given in Table 3.6. In particular, the elastic moduli have values comparable with those obtained on masonry of similar structural types. It should also be noted that torsional modal frequencies are underestimated by the model which, being of a lower order, is not perfectly verified. In fact, a calibration process extended to include the torsional mode, of reliable attribution, was not successful.

With the aid of the updated model, it was possible to complete the direct identification process on the higher frequency (Table 3.5). Furthermore, the model made it possible to classify the identified frequencies. Figure 3.5 shows one of the 13 modes identified by the proposed technique. At this second stage, the low coefficient of modal participation explained the total absence of some of these modal components in PSD

diagrams. In a further sensitivity study, it was seen that the restraint parameters have a negligible effect on lower modes [108], but in the field of frequencies of over 10 Hz, the bell tower loses its predominant influence on the modes, as the church building it is connected to prevails, so that mode classification calls for a global model reflecting the interaction between these two structural elements. A damage assessment stage would require the introduction of further local stiffness parameters in the calibration process.

The repair consisted of mortar injections and prestressed cables at each landing level. The results of new test campaign on SS. Annunziata tower [108], after a repair intervention, are summarized and compared with the original ones (Table 3.5 and table 3.6). One may notice the splitting effect on the two fundamental frequencies, already reported on repaired structures and due probably to non-linearity.

There was a 20-30% increase in the flexural frequencies (Young modulus) and a slight decrease in the torsional one (shear modulus). Thus, we can draw the following conclusions:

- a slight increase in *G,* probably a fictitious effect of the mass increase, show that the tower's shear behaviour has not significantly changed;
- a considerable increase in the Young modulus and bending stiffness demonstrates the efficacy of the intervention.

	Before repair		**After repair**	
Mode	**Measured frequencies (Hz)**	**Model frequencies (Hz)**	**Measured frequencies (Hz)**	**Model frequencies (Hz)**
1	1.66	1.67	1.97 2.12	1.97
2	2.26	2.25	2.34 2.54	2.54
3	4.67	3.86	4.30	4.00
4	6.18	5.96		6.70
5	6.40	6.55		7.33
6	8.90	7.45		7.98

Table 3.5 - Annunziata: identified and updated model frequencies, before and after the repair.

Updated parameters	**Before repair**	**After repair**
E	$12.3 \cdot 10^8$ N/m^2	$18.8 \cdot 10^8$ N/m^2
G	$2.5 \cdot 10^8$ N/m^2	$2.0 \cdot 10^8$ N/m^2
*G**	$0.2 \cdot 10^8$ N/m^2	$0.3 \cdot 10^8$ N/m^2

Table 3.6 - SS. Annunziata: parameters of the updated model.

3.3.3 Application to the Bell-Tower of Alba's Cathedral

A second test campaign regarded the bell tower of Alba's Cathedral (Figure 3.7) in the context of a rehabilitation intervention coordinated by Prof. Giuseppe Pistone. The tower has been subjected to an experimental investigation under three types of excitation: ambient vibrations, bell tolling and actions induced by a corer.

Acceleration measurements were carried out on the bell tower only, by placing three accelerometers per landing, arranged along the two horizontal axes. Two set-up were used, each one made up of the signals relating to 12 acquisition channels, of which three were fixed at the top level (43 m height) as reference channels and ten were moved to different landings. The measurements were made contemporarily in the E-W and N-S directions and the three fixed channels allowed correlating different set-up and building spatial modal shapes. During the signal pre-processing stage it was observed that the signals picked up under corer excitation were noisy and disturbed by strong harmonic components, hence they were not used in the elaborations.

Figure 3.7 - S. Lorenzo Cathedral bell-tower in Alba

The signals were analysed applying two different methods. The first one, in the time domain, is based on the ERA algorithm [109] applied on the estimated Random Decrement functions [26]. The second one, referred to as TFIE method, was applied by choosing Choi-Williams transforms with kernel parameter σ=5. ERA and TFIE methods were applied to different measurements, this resulting in occurrence diagrams for modal frequencies as depicted in Figure 6.

For brevity's sake, only a part of the identified modes is presented in Table 4, where the results coming from the two techniques may be compared. The first evident advantage in using TFIE was the possibility to work on several parameters (kernel selectivity, type of transform, etc.) that may improve the estimators and filter spurious components, as well as check modal energy changes in time. If compared to the previous application, the connection to the church in this case seems to play a more important role on the torsional components of the tower's modal shapes. A further proof of this influence is that the TFIE method has identified additional modes, here omitted for brevity's sake, that have been attributed to the church. On the other hand, the subspace and RD based algorithms showed to be more suitable when one has to perform a fast identification or when the system's dynamic behaviour is very clear.

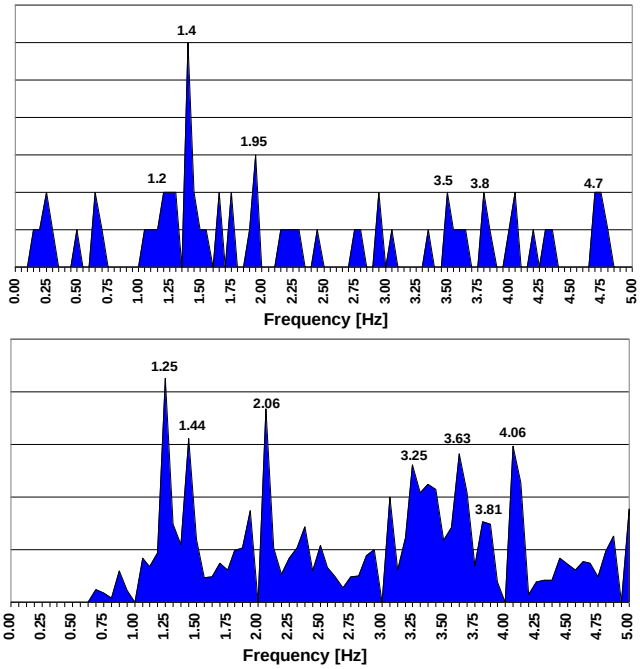

Figure 3.8 - S. Lorenzo Cathedral bell-tower: occurrence of modal frequency values resulting from different identification sessions

Mode	**1st**	**2nd**	**3rd**	**4th**	**5th**
TFIE frequencies [Hz]	1.25	1.44	3.63	3.81	4.12
ERA frequencies [Hz]	1.22	1.44	3.58	3.80	4.05

Table 3.7 - S. Lorenzo Cathedral bell-tower. Modal frequencies as identified through the TFIE method

3.3.4 Application to the dome of S.Gaudenzio in Novara

The dome of S. Gaudenzio Church in Novara (see Figure 3.9a) is a 117.5 m high monument, erected between 1844 and 1880 by Alessandro Antonelli, and represents one of the most daring masonry structures ever built. In view of its history, the past interventions and the current state of preservation, this dome is representative of a broad class of problems concerning historical structures.

From a structural standpoint, it is organized as follows: the pillars along the transept support (level 17.0 m) a series of arches, consisting of four lower and four upper arches which bear the first tambour (level 35.0 m). This consists of two outer series of columns resting on the upper arches and an internal series resting on the lower arches. Above the first tambour (level 53.0 m) the building splits in an inner and an outer structure. The outer one continues into a second tambour and, above this (level 67.0), up to a ribbed shell dome known as *gran tazza (big cup)*. Internally, the structure continues

into a hollowed dome ending in a cylindrical arrangement of columns that, in turn, supports (level 85.0 m) the 32 m high upper spire. The outer and the inner parts are mutually connected at many levels by means of arches and radial platbands.

The dome exhibited stability phenomena immediately after its completion, causing an uninterrupted sequence of maintenance and strengthening interventions. In the period between 1930 and 1946, reinforced concrete was extensively used to rebuild the original upper spire; the upper part of its masonry supporting structure was encased in concrete as well; steel ties and a concrete ring were installed at the dome impost level, with the scope of preventing a feared base arc collapse.

In a measurement campaign, the dome has been instrumented with 16 accelerometers, arranged along 4 levels, as shown in Figure 3.9a. The measurement direction is horizontal and tangent to the section perimeter for all the accelerometers, in order to detect torsional mode shapes. Signals have been acquired utilizing ambient vibration as excitation source, thus requiring the employment of output-only analysis techniques, as hereinafter described.

The Frequency Domain Decomposition (FDD) [40] and the TFIE techniques have been applied to a set of 500-second long ambient vibration records of the dome. It was observed that the FDD approach, applied to certain records, is unable to uncouple the first pair of modes. However, the failed uncoupling is evident from the complexity of the mode shape. Also the ERA method seemed to be incapable of decoupling clustered modes in the present case: this is also evident by the apparent high complexity of the associated eigenvalues. The outcomes of the identification are collected in table 3.8: it can be observed that both the FDD and the TFIE methods yield rather close values which also qualitatively agree with the preliminary FE prediction shown in figure 3.10. For the first mode, the FDD method yielded a shape similar to that of the preliminary FE model (see figure 3.10), while the TFIE method exhibited a mode dominated by shear deformability, i.e. governed by the bottom part of the structure.

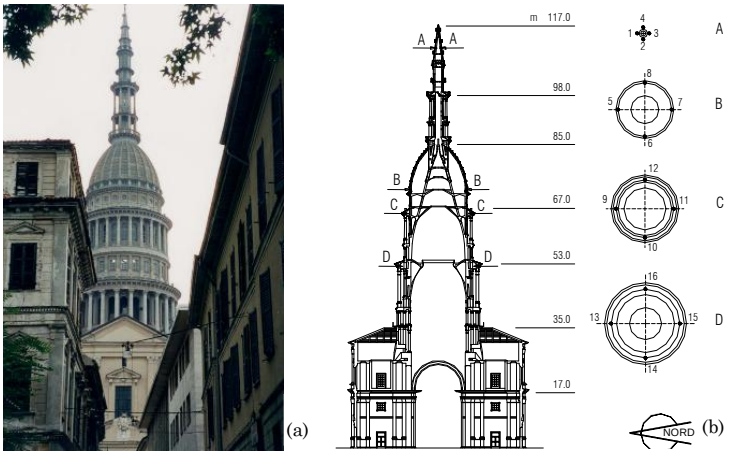

Figure 3.9 - The dome of S. Gaudenzio Church: overall view (a), and cross section (b).

Conversely, for the first torsional mode (1.77 Hz), the TFIE method showed a behaviour in close agreement with that of the model, with in phase rotations, unlike the FDD method. The other modal shapes, here omitted for brevity, were found to be more consistent, except for a number of alleged phase problems on the channels located on top.

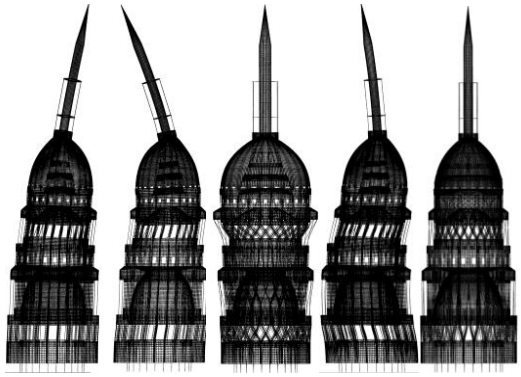

Figure 3.10 - Graphical representation of the mode shapes obtained through a FE model.

Mode	FDD frequencies [Hz]	TFIE frequencies [Hz]
1° - Bending	0.79	0.79
	0.81	0.82
2° - Bending	1.63	1.61
	1.67	1.67
1°- Torsional	1.73	1.77

Table 3.8 - Frequencies provided by the identification techniques.

The discrepancies may be ascribed to several factors which need to be examined more closely, including: (1) the use of different measuring sets for the two methods (only one set has been used for the TFIE method so far); (2) the structure complexity, whose behaviour is affected by the interaction between two structural systems (external and internal skeleton as shown in figure 3.9); (3) the interaction with the bottom part of the structure.

The FE model shown in figure 3.10 was built to reproduce the portion of the dome above level 26.5 m (i.e. just above the supporting arches of the transept) utilizing 53696 elements comprising beams and shells. The data used to update the model were essentially the frequencies collected in table 3.8 and the calibration process consisted of minimising a cost function based only on modal frequencies.

At a first stage, the unknowns of the calibration process boiled down to the masonry elastic modulus, the density and the Poisson ratio. With the aid of the updated model, it was possible to complete the direct identification process through the TFIE method on the higher frequencies (see Figures 9-10 and Table 6). Furthermore, the model made possible to classify the identified frequencies. With regard to frequencies and modal shapes the agreement between the six additional modes identified and those provided by modelling was good.

The better performance of the identification technique on high modes suggests that the current FE model were unable to fully reproduce all the phenomena governing the lowest modes, such as the restraint conditions between the different parts of the structure and the interaction with the bottom part of the basilica.

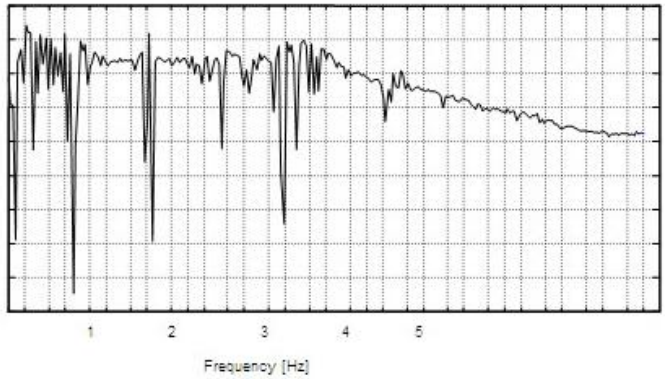

Figure 3.11 - Standard Deviation of a sample Phase Difference estimator (TFIE method).

	Frequencies [Hz]		
Mode	**Experimental (TFIE)**	**FE**	**Updated FE (final)**
2° - Torsional	2.92	2.76	2.88
3° - Bending	2.62	2.80	2.66
	2.99	2.80	2.66
3° - Torsional	3.38	3.46	3.33
4° - Bending	4.63	4.61	4.63

Figure 3.12 - Frequencies provided by the identification techniques compared with the updated model outcomes.

On the basis of the identified modes a model updating process was performed on the model in which additional side springs and extra masses at the base where added to simulate the interaction with the bottom part of the basilica.

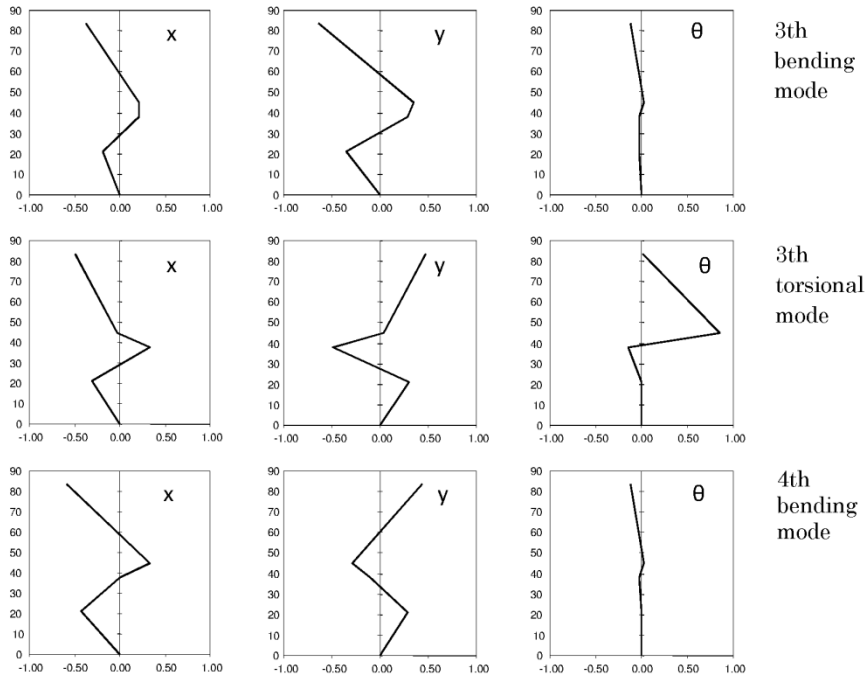

Figure 3.13 - Graphical representation of the higher modes obtained through the TFIE method (translations along the axes x and y and rotation angle θ respectively).

The parameters of this optimisation process were: the masonry elastic modulus and the Poisson ratio as well as the elastic modulus of the column granite (final value of the parameters were: E_m=3.7918e10 N/m²; ν_m=0.17; E_g=3.5e10 N/m²). The frequencies of the calibrated model (0.79, 0.80, 1.51, 1.55, 1.67 Hz; see Table 6 for the higher ones) show that the current model is unable to match the experimental ratio between the bending modes. This implies that the present FE model is not fully verified.

In this example different techniques provided results that are unreliable in some cases, and the evidence of this inconsistency only arose from the comparison among different methods and with the support of a well-conceived FE model of the dome. We conclude that the blind application of input-unknown techniques may result in misleading conclusions. Indeed, no method is capable of providing information that is not contained in the signal, independently on how refined the method can be.

3.3.5 Application to the Matilde's tower in San Miniato

The Torre di Matilde (Figure 3.14), erected in San Miniato (Pisa) in the 12th century, is a rare example of the military architecture of the time: its construction dates back to when the Emperor Henry IV (1184-1194) visited the city. The structure, including the bell tower, was badly damaged by the bombings of 1944.

The tower, rising ca 35 m above the cathedral floor, is parallelepiped shaped, with crown and end shrines added in the 13th century. Inside the tower, three wooden storeys prove too weak to ensure a valid connection between the four walls. At the top of the tower, a small masonry vault closes the structure by linking together the side walls. The cracking pattern of the building displays major lesions at the corners, extending over virtually the entire height. An extensive measuring campaign was performed on the tower, within the framework of an inter-university scientific program (PRIN).

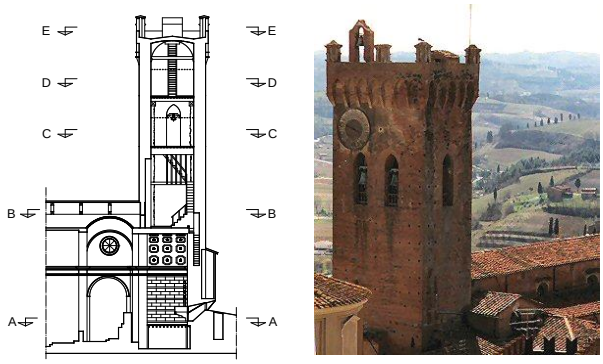

Figure 3.14 - View of the Torre di Matilde of S.Miniato (Pisa)

The results discussed in what follows refer in particular to dynamic response signals to environmental conditions acquired by means of 23 accelerometers (Figure 3.14), of which 10 were positioned on the parapet of the roofing (level E), 10 at the next to the last level (level D) and the remaining 3 at the level underneath (level C). Measuring directions were parallel to the main axes of the cross section of the building.

Different recorded segments were analysed, most of them obtained at a sampling frequency of 1.6 kHz. A preliminary qualitative analysis with Welch window energy spectra and representations in the joint time-frequency domain revealed important shares of spectral energy localised around three prevalent frequencies: 2.70 Hz, 3.40 Hz and 6.40 Hz. The analysis of a certain number of signals also revealed the presence of less pronounced peaks around the frequencies of 2.95 Hz, 4.70 Hz and 6.05 Hz. The energy spectrum in figure 3.15 summarises the frequencies recurring in most signals.

Structural identification was performed by using two time domain methods, ERA and PRTD, whose extension to environmental type signals required the prior extraction of the Random Decrement functions. Then time-frequency identification was performed through the TFIE method.

This study was limited to the analysis of vibration modes with frequencies lower than 10Hz; in this range, all methods identified a considerable number of modes, which invariably included modes associated with the frequencies already observed in the preliminary analysis. Table 3.9 lists the modal frequency values corresponding to the three principal modes obtained with the three methods by averaging the results over the various recorded segments analysed.

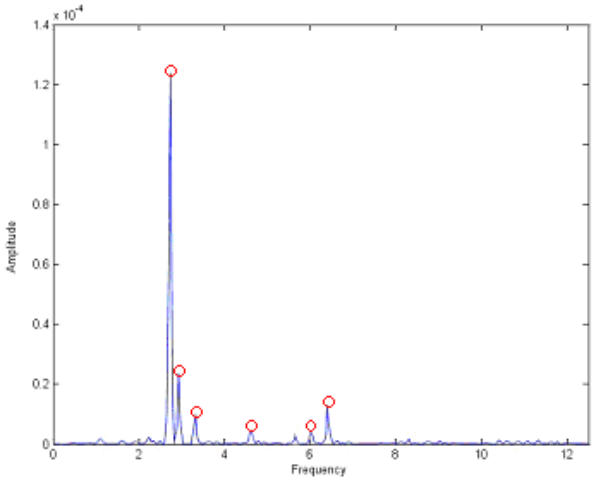

Figure 3.15 - Energy spectrum of a typical signal

ERA	PRTD	TFIE
2.6880 Hz	2.7036 Hz	2.7344 Hz
3.4109 Hz	3.4086 Hz	3.3913 Hz
6.3274 Hz	6.3538 Hz	6.3232 Hz

Table 3.9 - Modal frequencies identified with the various methods

Figure 3.16 and figure 3.17 show two sample diagrams of phase difference estimators (TFIE method), calculated on pairs of signals measured according to each of the two main directions. The concomitance of the main frequencies along the two orthogonal axes demonstrates that all the modes are affected by appreciable oblique and torsional components, an effect determined by the markedly asymmetrical configuration of the plan.

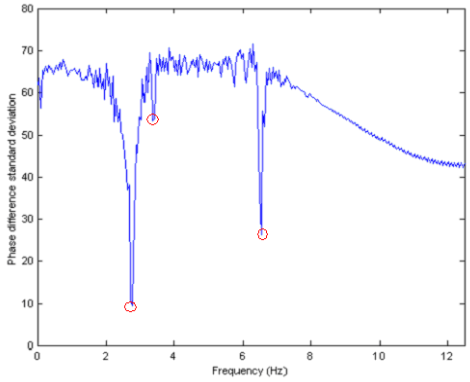

Figure 3.16 - Phase difference estimator – Sensors arranged along the Y axis

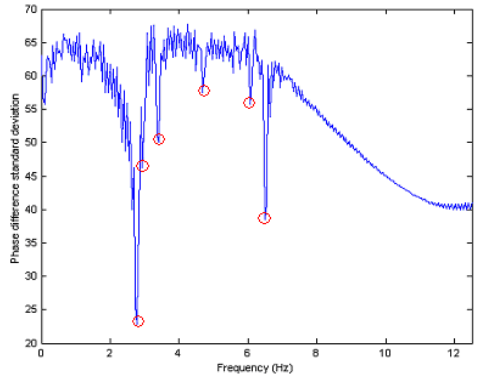

Figure 3.17 - Phase difference estimator – Sensors arranged along the X axis

The damping values obtained from the analyses in the time domain were seen to be affected by considerable scatter and, as already observed in earlier studies on "output only" methods, should be considered with some caution. Accordingly, these results have been omitted waiting for a more accurate, and more painstaking, evaluation by means of instantaneous damping estimators.

As for mode shapes, it was decided to represent them on a preliminary basis with vectors having their origins coinciding with the positions of the sensors and intensity and direction defined by the modules and phases of the eigenvectors, respectively (Figure 15). This made it possible to check the directions, which, in some segments, sometimes turned out to be reversed due to phase evaluation problems. This type of difficulty is very frequent in the identification of masonry buildings, on account of the non-linear behaviour of the materials, as well as structural complexity. To obviate phase problems, especially between channels acting in orthogonal directions, in addition to spatial analyses, separate analyses were performed in the two orthogonal directions.

The first vibrating mode is flexural in the lower stiffness plane. Once this mode has been identified, from the analysis of its associated eigenvector (Figure 3.18, figure 3.19) it can be seen that the top storey of the tower does not only translate but it also has a pronounced rotational component; this rotational behaviour of the top floor was also brought out by the analysis performed in the orthogonal direction (X). By averaging the different results a modal shape of a basic translational type in the lower stiffness plane was obtained.

Figure 3.19 also illustrates the other two principal modes determined with the ERA method, i.e., a mode characterised by prevalent translation along the greater stiffness direction X (also showing a strong torsional effect at the top level) and a predominantly torsional mode.

The shapes corresponding to the other frequencies identified were also constructed, but, in view of their weak energy and complexity, they could not be classified. A simplified, non-calibrated model, worked out with the ADINA code, has led to preliminary hypotheses about the frequency around 2.95Hz, which might be associated

with the first mode of the roof vault, whilst the other frequencies might be either modes associated with the adjacent church or ovalisation or wall modes. The latter might fall within a relatively low frequency range owing to the weakening effect of the cracks along the corners of the tower.

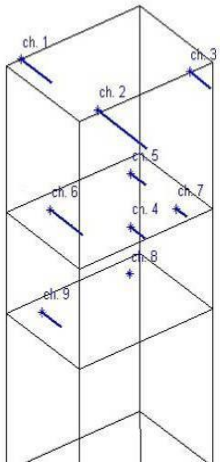

Figure 3.18 - First identification mode determined with the ERA method – Prevalent translation in the lower stiffness plane (Y direction)

The model also yields a ratio, of ca 1.20, between the frequencies of the first translational modes in the two directions, in good agreement with the ratio determined experimentally, of 1.25.

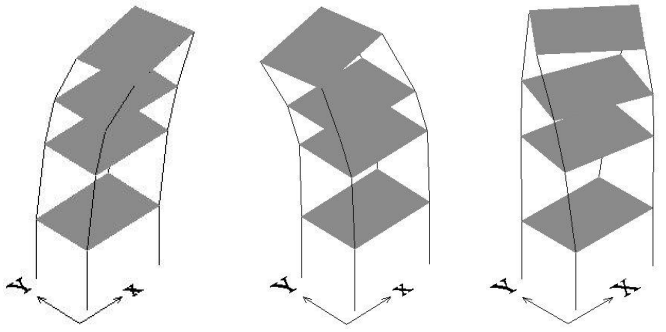

(a) Mode 1 (2.7 Hz) (b) Mode 3 (3.4 Hz) (c) Mode 5 (6.4 Hz)

Figure 3.19 - The three modes identified reliably.

References

[1] Natke, H.G., Tomlinson, G.R., Yao, J.T., (1993); *Safety evaluation based on identification approaches*, Braunschweig/Weisbaden Vieweg & Sohn.

[2] Ghanem, R., Shinozuka, M., (1995); *Structural system identification II: Experimental verification*. ASCE J. of Eng. Mech., 121(2), pp. 265-273.

[3] Maia, N.M.N., Silva, J.M.M., (1997); *Theoretical and experimental modal analysis*, Research Studies Press, Wiley.

[4] Van Der Auweraer, H., (2002); *Testing in the age of virtual prototyping*. Proceedings of International Conference on Structural Dynamics Modelling, Funchal.

[5] Soderstrom, T., Stoica, P., (1989); *System identification*, Englewood Cliffs.

[6] Ewins, D.J., (2000); *Modal testing*, Research Studies Press Ltd.

[7] Heylen, W., Lammens, S., Sas, P., (1997); *Modal Analysis Theory and Testing*, Leuven KUL Press.

[8] Shinozuka, M., Yum, C.B., Imai, H., (1982); *Identification of linear structural dynamic systems*. ASCE Journal of Engineering Mechanics, 108(6), pp. 1371-1390.

[9] Natke, H.G., Yao, J.T.P., (1986); *Research topics in structural identification*. Proceedings of 3rd Conference on dynamic response of structures ASCE, New York, pp. 542-550.

[10] Safak, E., (1991); *Identification of linear structures using discrete-time filters*. ASCE Journal of Structural Engineering, 117(10), pp. 3064-3085.

[11] Safak, E., Celebi, M., (1991); *Seismic response of transamerica building. II: System-identification*. ASCE Journal of Structural Engineering, 117(8), pp. 2405-2425.

[12] Peeters, B., DeRoeck, G., (1999); *Reference-based stochastic subspace identification for output-only modal analysis*. Mechanical Systems and Signal Processing, 13, pp. 855-878.

[13] Loh, C.H., Lin, C.Y., Huang, C.C., (2000); *Time domain identification of frames under earthquake loadings*. ASCE Journal of Engineering Mechanics, 126(7), pp. 693-703.

[14] Ljung, L., (1999); *System identification theory*, Prentice Hall.

[15] Fassois, S.D., Lee, J.E., (1993); *On the problem of stochastic experimental modal analysis based on multiple-response data. Part II: the modal analysis approach*. Journal of Sound and Vibrations, 161(1), pp. 57-87.

[16] Ibrahim, S.R., Mikulcik, E.C., (1977); *A method for the direct identification of vibration parameters from the free response*. The shock and vibration bulletin, 47(4), pp. 183-198.

[17] Juang, J.N., Pappa, R.S., (1984); *An eigensystem realisation algorithm (ERA) for modal parameter identification and modal reduction*. NASA/JPL Workshop on identification and control of flexible space structures.

[18] Lew, J.S., Juang, J.N., Longman, R.W., (1993); *Comparison of several system identification methods for flexible structures*. Journal of Sound and Vibrations,

167(3), pp. 461-480.

[19] Vold, H., Kundrat, J., Rocklin, G.T., Russel, R., (1982); *A multi-input modal estimation algorithm for mini-computers*. SAE Paper number 820194.

[20] Deblauwe, F., Allemang, R.J., (1985); *The polyreference time domain technique*. Proceedings of the 10th International Seminar on Modal Analysis, Katholieke.

[21] Zeiger, H.P., McEwewn, A.J., (1974); *Approximate linear realisations of given dimension via Ho's algorithm*. IEEE Transactions on Automatic Control, 153.

[22] James, G.H., Carne, G.T., Lauffer, J.P., (1995); *The natural excitation tecnique (NexT) for modal parameter extraction from operating structures*. Modal Analysis, 10, pp. 260-277.

[23] Van Overschee, P., De Moor, B., (1996); *Subspace Identification for Linear Systems: Theory and Implementation - Applications*, Kluwer Academic Press Dordrecht.

[24] Leuridan, J.M., Brown, D.L., Allemang, R.J., (1985); *Time domain parameter identification methods for linear modal analysis: a unifying approach*. ASME Paper Number 85-DET-90.

[25] Giorcelli, E., Fasana, A., Garibaldi, L., Riva, A., (1994); *Modal analysis and system identification using ARMAV models*. Proceeding of 12th International Modal Analysis Conference IMAC, Honolulu, pp. 667-680.

[26] Asmussen, J.C., (1997); *Modal Analysis based on Random Decrement Technique*. Aalborg University, PhD Thesis.

[27] Brincker, R., Krenk, S., Jensen, J.L., (1991); *Estimation of correlation functions by the random decrement technique*. Proceedings of 9th Internatiopnal Modal Analysis Conference and Exhibit, Florence.

[28] Golub, G.H., Van Loan, C.F., (1983); *Matrix Computations*, The Johns Hopkins University Press.

[29] Larimore, W.E., (1990); *Canonical Variate Analysis*. Proceedings of the 29th IEEE Conference on Decision and Control, Honolulu, Hawaii, pp. 635-639.

[30] Capecchi, D., D'Ambrogio, W., (1993); *Experimental modal analysis and damage detection on an ancient masonry building*. Meccanica, 28, pp. 13-25.

[31] Richardson, C.M., Formenti, D.L., (1982); *Parameter Estimation from Frequency Response measurements using rational fraction polynomials*. Proceedings of the 1st International Modal Analysis Conference (IMAC I), Orlando, pp. 167-181.

[32] Genovese, F., Antonacci, E., Vestroni, F., (1997); *Caratterizzazione dinamica di una casa in muratura*. Atti del VIII Convegno nazionale ANIDIS - L'ingegneria sismica in Italia, Taormina, pp. 503-510.

[33] Beolchini, G.C., Antonacci, E., (2001); *Il comportamento dinamico di S.Maria di Collemaggio: previsioni numeriche e osservazioni sperimentali*. Atti del X Convegno nazionale ANIDIS - L'ingegneria sismica in Italia, Potenza-Matera.

[34] Goyder, H.G.D., (1980); *Methods and Applications of Structural Modelling from measured frequency response data*. Journal of Sound and Vibration, 68(2), pp. 209-230.

[35] Beni, F., Lagomarsino, S., Marazzi, F., Magonette, G., Podestá, S., (2002); *Structural*

monitoring through dynamic identification. Proceedings of the 3rd World Conference on Structural Control, Chirchester, pp. 139-146.

[36] Binda, L., Saisi, A., Tiraboschi, C., (2000); *Investigation procedures for the diagnosis of historic masonries*. Construction and building materials, 14, pp. 199-233.

[37] Slavik, M., (2002); *Assessment of bell towers in Saxony. Structural Dynamics*. Eurodyn 2002.

[38] Zabel, V., Bucher, C., (2003); *Experiences with dynamic investigations of historica bell towers and belfries*. Proceedings of IMAC-XXI, International Modal Analysis Conference, Kissimmee, pp. 1244-1250.

[39] Cuadra, C., Karkee, M.B., Tokeshi, K., (2008); *Earthquake rish to Inca's historical constructions in Machupicchu*. Advances in Engineering Software, 39(4), pp. 336-345.

[40] Brincker, R., Lingmi, Z., Palle, A., (2001); *Modal identification of output-only systems using frequency domain decomposition*. Smart Materials and Structures, 10, pp. 441-445.

[41] Cohen, L., (1995); *Time-Frequency Analysis*, Englewood Cliffs, NJ Prentice-Hall Inc.

[42] Hlawatsch, F., Boudreaux-Bartels, G.F., (2006); *Linear and quadratic time-frequency signal representations*. IEEE Signal Processing Magazine, 20, pp. 1483-1510.

[43] Ceravolo, R., (2004); *Use of instantaneous estimators for the evaluation of structural damping*. J. of Sound and Vib., 274(1-2), pp. 385-401.

[44] Spina, D., Valente, C., Tomlinson, G.R., (1996); *A new procedure for detecting nonlinearity from transient data using the Gabor transform*. Nonlinear Dynamics, 11(3), pp. 235-254.

[45] Gabor, D., (1946); *Theory of communication*. Journal of the IEE (London), 93, pp. 429-457.

[46] Feichtinger, H.H., Strohmer, T., (1998); *Gabor Analysis and Algorithms: Theory and Applications*, Birkhauser.

[47] Carmona, R., Hwang, W.L., Torrésani, B.P., (1998); *Practical time-frequency analysis*, San Diego, CA 92101-4495, USA Academic Press.

[48] Newland, D.E., (1999); *Ridge and phase identification in the frequency analysis of transient signals by harmonic wavelets*. Journal of Vibration and Acoustics, 121, pp. 149-155.

[49] Erlicher, S., Argoul, P., (2007); *Modal identification of linear non-proportionally damped systems by Wavelet transform*. Mech. Sys. and Signal Process., 21(3), pp. 1386-1421.

[50] Hammond, J.K., Waters, T.P., (2001); *Signal processing for experimental modal analysis*. Philosophical Transactions of the Royal Society A, 359(1778), pp. 41-59.

[51] Sohn, H., Farrar, C.R., Hemez, F.M., Shunk, D.D., Stinemates, D.V. et al., (2003); *A review of structural health monitoring literature: 1996-2001*. Los Alamos National Laboratory Report LA-13976-MS.

[52] Loughlin, P.J., Pitton, J.W., Atlas, L.E., (1993); *Bilinear time-frequency*

representations: new insights and properties. IEEE Transactions on Signal Processing, 41, pp. 750-766.

[53] Claasen, T.A., Mechlenbrauker, W.F., (1980); *The Wigner distribution - a tool for the time-frequency analysis; part III: relations with other time-frequency signal transformations*. Philips Journal of Research, 35, pp. 372-389.

[54] Mecklenbrauker, W.F., Hlawatsch, F., (1997); *The Wigner Distribution: Theory and Applications in Signal Processing*, Amsterdam Elsevier.

[55] Martin, W., Flandrin, P., (1989); *Wigner-Ville spectral analysis of non-stationary processes*. IEEE Transactions on Signal Processing, 33, pp. 1461-1470.

[56] Flandrin, P., Martin, M., (1997); The Wigner-Ville spectrum of nonstationary random signals, in: Mecklenbrauker, W.F., Hlawatsch, F., *The Wigner Distribution: Theory and Applications in Signal Processing*, Amsterdam, pp. 211-267.

[57] Janssen, A.J., (1997); Positivity and spread of bilinear time-frequency distributions, in: Mecklenbrauker, W.F., Hlawatsch, F., *The Wigner Distribution: Theory and Applications in Signal Processing*, Amsterdam, Elsevier, pp. 1-58.

[58] Mallat, S., Papanicolau, G., Zhang, Z., (1998); *Adaptive covariance estimation of locally stationary processes*. The Annals of Statistics, 28, pp. 1-47.

[59] Dahlhaus, R., (1997); *Fitting time series models to nonstationary processes*. The Annals of Statistics, 25, pp. 1-37.

[60] Ceravolo, R., (2009); Time-frequency analysis, in: Boller, C., Chang, F.K., Fujino, Y., *Encyclopedia of Structural Health Monitoring*, Chirchester, UK, Wiley & Sons Ltd, ch. 26.

[61] Kozek, W., (1996); *Time-frequency signal processing based on the Wigner-Weyl framework*. Signal Processing, 29, pp. 77-92.

[62] Priestley, M.B., (1967); *Power spectral analysis of non-stationary random processes*. J. of Sound and Vib., 6(1), pp. 86-97.

[63] Dalianis, S.A., Hammond, J.K., White, P.R., Cambourakis, G.B., (1998); *Simulation and identification of nonstationary systems using linear time-frequency methods*. Journal of Vibration and Control, 4, pp. 75-91.

[64] Hammond, J.K., White, P.R., (1996); *The analysis of non-stationary signals using time-frequency methods*. J. of Sound and Vib., 190(3), pp. 419-447.

[65] Bonato, P., Ceravolo, R., De Stefano, A., Molinari, F., (2000); *Use of cross time-frequency estimators for the structural identification in non-stationary conditions and under unknown excitation*. J. of Sound and Vib., 237(5), pp. 775-791.

[66] Bonato, P., Ceravolo, R., De Stefano, A., Molinari, F., (2000); *Cross time-frequency techniques for the identification of masonry buildings*. Mechanical Systems and Signal Processing, 14, pp. 91-109.

[67] De Stefano, A., Matta, E., Quattrone, A., (2009); *Improvement of Time-Frequency domain identification through PCA*. Proceedings of IOMAC09 3rd International Modal Analysis Conference, Ancona, Italy.

[68] Cohen, L., (1989); *Time-frequency distribution: a review*. Proceedings of the IEEE, 77, pp. 941-981.

[69] Boudreaux-Bartels, G.F., Parks, T.W., (1986); *Time-varying filtering and signal estimation using Wigner distribution synthesis techniques*. IEEE Transactions on Acoustics Speech and Signal Processing, 34, pp. 442-451.

[70] Ceravolo, R., Demarie, G.V., Erlicher, S., (2007); *Instantaneous Identification of Bouc-Wen-type Hysteretic Systems from Seismic Response Data*. Key Eng. Mater., 347, pp. 331-338.

[71] Zhang, Q.W., Chang, T.Y.P., Chang, C.C., (2001); *Finite element model updating for the Kap Shui Mun cable-stayed bridge*. Journal Bridge Engineering,(6), p. 285.

[72] Brownjohn, J.M.W., Lee, J., Cheong, B., (1999); *Dynamic performance of a curved cable-stayed bridge*. Engineering structures,(21), pp. 1015-1027.

[73] Guyan, R., (1965); *Reduction of Stiffness and Mass Matrices*. AIAA Journal, 3(2), p. 380.

[74] Zhang, N., (1995); *Dynamic condensation of mass and stiffness matrices*. Journal of Sound and Vibration, 188(4), pp. 601-615.

[75] O'Callahan, J., (1989); *A new procedure for and Improved Reduced System (IRS)*. IMAC VII, Las Vegas.

[76] O'Callahan, J., Avitabile, P., Riemer, R., (1989); *System Equivalent Reduction Expansion Process (SEREP)*. IMAC VII, Las Vegas.

[77] Friswell, M.I., Mottershead, J.E., (1995); *Finite Element Model Updating in Structural Dynamics*, Kluwer Academic Publishers.

[78] Berman, A., Nagy, E.J., (1983); *Improvement of large analytical model using test data*. AIAA Journal 21, 8, pp. 1168-1173.

[79] Caesar, B., (1986); *Update and identification of dynamic mathematical models*. IMAC IV, pp. 394-401.

[80] Baruch, M., Bar-Itzhack, I.Y., (1978); *Optimal weighted orthogonalization of measured modes*. AIAA Journal 16, 4, pp. 346-351.

[81] Wei, F.S., (1990); *Structural dynamic model improvement using vibration test data*. AIAA Journal 28, pp. 175-177.

[82] Minas, C., Inman, D., (1988); *Correcting finite element models with measured modal results using eigenstructure assignment methods*. International Modal Analysis Conference, Kissimmee, pp. 583-587.

[83] Gladwell, G.M.L., (1986); *Inverse Problems in Vibration*, Dordrecht Springer.

[84] Kirkpatrick, S., Gelatt, C.D., Vecchi, M.P., (1983); *Optimization by Simulated Annealing*. Science, 1(220), pp. 671-680.

[85] Johnson, D.S., Aragon, C.R., Schevon, L.A., (1989); *Optimization by Simulated Annealing: an Experimental evaluation*. Graph Partitioning, pp. 365-392.

[86] Srinivas, M., Patnaik, L.M., (1994); *Genetic algorithms: a survey*. IEEE Computer Magazines, pp. 17-24.

[87] Dack, T.B., Hoffmeistert, F., Schwefel, H.P., (1991); *A survey of evolutionary strategies*. Proceeding of the international conference of Genetic Algorithms, San Diego.

[88] Christodoulou, K., Ntotsios, E., Papdimitriou, C., Panetsos, P., (2008); *Structural model updating and prediction variability using Pareto optimal models*. Computer Methods in Applied Mechanics and Engineering, 198, pp. 138-149.

[89] Wittrick, W.H., (1962); *Rates of change of eigenvalues, with reference to buckling and vibration problems*. Journal of the Royal Aeronautical Society, 66, pp. 590-591.

[90] Fox, R.L., Kapoor, M.P., (1968); *Rates of Change of Eigenvalues and Eigenvectors*. AIAA Journal, 6(12), p. 2426.

[91] Allemang, R.J., (2002); *The Modal Assurance Criterion (MAC): twenty years of use and abuse*. IMAC.

[92] Bonato, P., Ceravolo, R., De Stefano, A., (1997); *Time-Frequency and ambiguity function approaches in structural identification*. J. of Eng. Mech., 123(12), pp. 1260-1267.

[93] Mares, C., Mottershead, J.E., Friswell, M.I., (2006); *Stochastic model updating: Part 1 - theory and simulated example*. Mechanical Systems and Signal Processing, pp. 1074-1095.

[94] Xiong, Y., Chen, W., Tsui, K.L., Apley, D.W., (2009); *A better understanding of model updating strategies in validating engineering models*. Computer methods in applied mechanics and engineering, pp. 1327-1337.

[95] Goller, B., Padlwarter, H.J., Schueller, G.I., (2009); *Robust model updating with insufficient data*. Computer methods in applied Mechanics and Engineering, 198, pp. 3096-3104.

[96] Govers, Y., Link, M., (2009); *Stochastic model updating - Covariance matrix adjustment from uncertain experimental modal data*. Mechanical Systems and Signal Processing, p. In press.

[97] Collins, J.D., Hart, G.C., Hasselman, T.K., Kennedy, B., (1974); *Statistical identification of structures*. AIAA Journal, 2, pp. 185-190.

[98] Beck, J.L., Katafygiotis, L.S., (1998); *Updating models and theirn uncertainties*. Journal of Engineering Mechanics, 124(4), pp. 455-461.

[99] Katafygiotis, L.S., Beck, J.L., (1998); *Updating models and their uncertainties*. Journal of Engineering Mechanics, 124(4), pp. 463-467.

[100] Neal, R.M., (1993); *Probabilistic inference using Markov chain Monte Carlo methods*. Department of Computer Science, University of Toronto, Technical Report CRG-TR-93-1.

[101] Marczyk, J., (1997); Meta-computing and computational stochastic mechanics, in: Marczyk, J., *Computational Stochastic Mechanics in a Meta-computing Perspective*, Barcelona, CIMNE.

[102] Fonseca, J.R., Friswell, M.I., Mottershead, J.E., Lees, A.W., (2005); *Uncertainty identification by the maximum likelihood method*. Journal of Sound and Vibration, 288, pp. 587-599.

[103] Ghanem, R.G., Spanos, P.D., (2003); *Stochastic Finite Elements: A Spectral Approach*, New York Dover.

[104] Ghanem, R., Red-Horse, J.R., (2000); *Modal properties of a space-frame with*

localised system uncertainties. Proceedings of the 8th ASCE Speciality Conference on Probabilistic Mechanics and Structural Reliability.

[105] Belouchrani, A., Abed-Meraim, K., Cardoso, J.F., Molines, E., (1997); *A BSS technique using 2nd-order statistics*. IEEE Transaction on Signal Processing, 45, pp. 434-444.

[106] Bendat, J.S., Piersol, A.G., (1980); *Engineering Application of Correlation and Spectral Analysis*, New York Wiley Interscience.

[107] De Stefano, A., Ceravolo, R., (2007); *Assessing the Health State of Ancient Structures: The Role of Vibrational Tests*. Journal of Intelligent Material Systems and Structures, 18, pp. 793-807.

[108] Ceravolo, R., Genovese, C., Pavese, A., Pistone, G., Zorgniotti, D., (1999); *Finalizzazione all'Intervento di Restauro dell'Identificazione Strutturale di una Torre Campanaria*. Proceedings IX Italian National Conference "L'Ingegneria Sismica in Italia" ANIDIS, Turin.

[109] Juang, J.N., (1994); *Applied System Identification*, New Jersey Prentice-Hall.